#### **Research Article**

Salah Al-Zubaidi, Jaharah A. Ghani, Che Hassan Che Haron, Adnan Naji Jameel Al-Tamimi, M. N. Mohammed\*, Alessandro Ruggiero, Samaher M. Sarhan, Oday I. Abdullah, and Mohd Shukor Salleh

# Investigation of the performance of integrated intelligent models to predict the roughness of Ti6Al4V end-milled surface with uncoated cutting tool

https://doi.org/10.1515/jmbm-2022-0300 received June 02, 2023; accepted August 31, 2023

Abstract: Titanium alloys are broadly used in the medical and aerospace sectors. However, they are categorized within the hard-to-machine alloys ascribed to their higher chemical reactivity and lower thermal conductivity. This aim of this research was to study the impact of the dry-end-milling process with an uncoated tool on the produced surface roughness of Ti6Al4V alloy. This research aims to study the impact of the dry-end milling process with an uncoated tool on the produced surface roughness of Ti6Al4V alloy. Also, it seeks to develop a new hybrid neural model based on the training back propagation neural network (BPNN) with swarm optimization-gravitation search hybrid algorithms (PSO-GSA). Full-factorial design of the experiment with L27 orthogonal array was applied, and three end-milling parameters (cutting speed, feed rate, and axial depth of cut) with three levels were selected (50, 77.5, and 105 m/min; 0.1, 0.15, and 0.2 mm/tooth; and 1, 1.5, and 2 mm) and investigated to show their influence on the obtained surface roughness. The results revealed that the surface roughness is significantly affected by the feed rate followed by the axial depth. A 0.49  $\mu m$  was produced as a minimum surface roughness at the optimized parameters of 105 m/min, 0.1 mm/tooth, and 1 mm. On the other hand, a neural network having a single hidden layer with 1–20 hidden neurons, 3 input neurons, and 1 output neuron was trained with both PSO and PSO–GSA algorithms. The hybrid BPNN–PSO–GSA model showed its superiority over the BPNN–PSO model in terms of the minimum mean square error (MSE) that was calculated during the testing stage. The best BPNN–PSO–GSA hybrid model was the 3–18–1 structure, which reached the best testing MSE of 3.8  $\times$  10 $^{-11}$  against 2.42  $\times$  10 $^{-5}$  of the 3–8–1 BPNN–PSO hybrid model.

**Keywords:** hybrid algorithm, uncoated tool, Ti6Al4V alloy, particle swarm–gravitational search algorithms, end milling

**Adnan Naji Jameel Al-Tamimi:** College of Technical Engineering, Al-Farahidi University, Baghdad, Iraq

**Alessandro Ruggiero:** Department of Industrial Engineering, University of Salerno, 84084 Fisciano, Italy

**Mohd Shukor Salleh:** Department of Manufacturing Engineering, Faculty of Industrial and Manufacturing Technology and Engineering, Universiti Teknikal Malaysia Melaka, Hang Tuah Jaya, 76100 Durian Tunggal, Melaka, Malaysia

<sup>\*</sup> Corresponding author: M. N. Mohammed, Mechanical Engineering Department, College of Engineering, Gulf University, Sanad 26489, Bahrain, e-mail: dr.mohammed.alshekhly@gulfuniversity.edu.bh Salah Al-Zubaidi: Department of Automated Manufacturing Engineering, Al-Khwarizmi College of Engineering, University of Baghdad, Baghdad 10071, Iraq; Mechanical Engineering Department, College of Engineering, Gulf University, Sanad 26489, Bahrain Jaharah A. Ghani, Che Hassan Che Haron: Department of Mechanical and Manufacturing Engineering, Faculty of Engineering and Built Environment, Universiti Kebangsaan Malaysia, 43600 Bangi, Selangor, Malaysia

**Samaher M. Sarhan:** Department of Mechatronics Engineering, Al-Khwarizmi College of Engineering, University of Baghdad, Baghdad 10071, Iraq

**Oday I. Abdullah:** Department of Energy Engineering, College of Engineering, University of Baghdad, Baghdad Iraq; Mechanical Engineering Department, College of Engineering, Gulf University, Sanad 26489, Bahrain

#### **Abbreviations**

worst(t)

Kbest

| BPNN                  | Backpropagation neural network                             |
|-----------------------|--|
| GSA                   | Gravitational search algorithm                             |
| GA                    | Genetic algorithm  |
| RSM                   | Response surface methodology                               |
| TS                    | Tabu search  |
| PSO                   | Particle swarm optimization                                |
| PSO-GSA               | Particle swarm optimization—gravitational                  |
|                       | search algorithm   |
| AC                    | Ant colony   |
| GP                    | Genetic programming  |
| SA                    | Simulated annealing  |
| ANFIS                 | Adaptive neuro-fuzzy inference system                      |
| ANN                   | Artificial neural network                                  |
| ABC                   | Artificial bee colony                                      |
| Xj                    | Input training vector                                      |
| Hk                    | Total hidden output  |
| Yz                    | Predicted output   |
| Tz                    | Real target  |
| $\delta z$            | Error of the output layer                                  |
| $\delta k$            | Error of the hidden layer                                  |
| α                     | Learning rate  |
| N                     | No. of agents  |
| $x_i^d Xid$           | Location of <i>i</i> th agent in the <i>d</i> th dimension |
| $F_{ij}d(t)$          | Force that acts on mass "i" from mass "j"                  |
| $M_{aj}$              | Active gravitational mass relevant to agent j              |
| $M_{pi}$              | Passive gravitational mass relevant to                     |
| •                     | agent i  |
| <i>G</i> ( <i>t</i> ) | Gravitational constant at time t                           |
| $\varepsilon$         | Small constant   |
| $R_{ij}(t)$           | Euclidian distance between two agents i                    |
|                       | and <i>j</i>   |
| $F_i d(t)$            | Total force acting on agent $i$ in a dimension             |
| rand <sub>j</sub>     | A random number in the interval [0, 1]                     |
| $a_i d(t)$            | Acceleration of the agent $i$ at time $t$ and in           |
|                       | direction <i>d</i> th                                      |
| $M_{ii}$              | Inertial mass of <i>i</i> th agent                         |
| Vid(t+1)              | Next velocity of the <i>i</i> th agent                     |
| Vid(t)                | Current velocity of the <i>i</i> th agent                  |
| Xid(t+1)              | Next position of the <i>i</i> th agent                     |
| Xid(t)                | Current position of the <i>i</i> th agent                  |
| G0                    | Initial value of the gravitational constant                |
| $fit_i(t)$            | Fitness value of the agent $i$ at time $t$                 |
| best(t)               | Max $fit_i(t)$ for minimization                            |
| *.*******(*)          | Min ft(t) for minimization                                 |

Min  $fit_i(t)$  for minimization

biggest mass

First *K* agents with the best fitness value and

#### 1 Introduction

The biomedical, energy, and aerospace industries are considered the main market for titanium alloys. Ti6Al4V alloy is widely used by those sectors due to its excellent properties. However, it is grouped within difficult-to-machine alloys because of poor thermal conductivity and large chemical reactivity. Annually, multiple tones of materials are converted to unutilized chips in various machining processes. This concern is quietly enlarged for such expensive materials that generate a huge press on the investigators and machinists.

Many researchers carried out various studies to evaluate the machinability of titanium alloy and find the optimal cutting conditions that maintain minimum surface conditions, cutting forces, and maximum tool life. For example, Ti6Al4V alloy was subjected to high-speed milling by Su *et al.* [1] in different environments, including flood, cold nitrogen at zero and hundred Celsius, cold and compressed nitrogen with oil mist, nitrogen with oil mist, and dry cutting. They aimed to extract the optimal settings for the uncoated carbide insert and revealed that flank wear was the most identified failure mode for all the applied environments.

When dry milling Ti6Al4V alloy using CVD-coated insert at different cutting speeds, complex wear mechanisms have been identified, according to Li *et al.* [2]. Due to mechanical loading, mechanical damage was detected at low cutting speeds, whereas high cutting speeds encouraged thermal damage, which in turn led to the major mechanisms of tool wear. Tool wear was discovered to be the critical factor that has the most bearing.

The performance of coated and uncoated carbide-cutting tools was examined by Elmagrabi *et al.* [3] for the endmilling Ti-6Al-4V alloys. The levels of feed rate, cutting speed, and depth of cut that have been implemented were 0.1, 0.15, and 2 mm/tooth; 50, 80, and 105 m/min; and 1, 1.5, and 2 mm respectively. They determined the tool life and surface roughness of both tools and found that the PVD tool performs better with 11.5 min and achieved finer surface than an uncoated tool.

The impact of milling parameters and insert wear on the surface finish of Ti6Al4V alloy was investigated by Safari *et al.* [4]. The necessary experiments were conducted using new and old TiAlN + TiNPVD-coated inserts with various speeds and feed rates (100–300 m/min, 0.03 and 0.06 mm/tooth). At larger cutting speeds, it was discovered that tool condition had a significant impact on surface roughness, with new inserts achieving 185 nm compared with older ones (320 nm). High levels of speed caused

plastic deformation in the sub-surface area, whereas high levels of feed rate caused surface quality degradation, especially at low cutting speeds.

The performance of liquid nitrogen (LN2) was explored by Zhao et al. [5] for its impact on surface integrity during the milling of Ti6Al4V alloy. The use of LN2 as a coolant resulted in high microhardness and compressive residual stresses as well as an improvement in surface quality over a temperature range of 20-196. No discernible difference was seen in grain size reduction as compared to dry milling. The effectiveness of cryogenic milling in improving surface integrity was proven by the authors.

The influence of Ti6Al4V alloys' microstructures (fine and larger equiaxed grains) on the cutting forces, surface roughness, and build-up edge during micro-end milling was examined by Ahmadi et al. [6]. Using the electron backscatter diffraction method, the microstructures of the endmilled surface were examined. According to the authors, fine-grain alpha plus beta with little  $\beta$  generated large levels of cutting forces. Additionally, the type of microstructure had an impact on how the build-up edge formed and its associated size.

To cut down on machining time and expenses, realistic models for predicting machining outputs should be developed. Based on prior studies, numerous researchers have tried and created a variety of ways to address these types of parameter optimization problems. These techniques involve classical and non-classical optimization algorithms. Particle swarm optimization (PSO), Tabu search, ant colony (AC), genetic programming, genetic algorithm (GA), simulated annealing, artificial neural network (ANN), and adaptive neuro-fuzzy inference system are among the popular artificial intelligence (AI) techniques that are claimed to be sufficiently general [7]. Neural networks, for instance, can be used in various disciplines and can take the role of extensive numerical simulation [8,9].

To optimize the end-milling parameters and estimate the surface quality of AISI 1040 plain carbon steel, an ANN model in conjunction with GA was constructed by Oktem et al. [10]. Analysis of variance (ANOVA) and multiple regression analysis were also used to investigate how cutting conditions affected surface roughness. The machining time was decreased to 20% at 3.27% error using the integrated method that was suggested.

During the milling of aluminium alloys, PSO was used by Bharathi Raja and Baskar [11] to anticipate the surface roughness. Based on these experimental data, an analytical model was developed to estimate surface roughness using PSO. The authors found that the limitations relating to both the experimental and theoretical methods were comparable to the real roughness.

Del Prete et al. [12] used response surface methodology (RSM) to create a surface roughness prediction model for flat-end milling. Surface roughness was estimated using ANN, but the surface roughness model was optimized using GA. The process parameters of the study were speed, depth of cut, feed rate, and radial engagement. The RSM was combined with GA to determine the best process variables resulting in a fine surface. Experiment results were used to verify the developed model where GA improved the surface roughness by 13 to 27%. The produced RSM model was possible to integrate with GA, and the effectiveness of the optimization process was primarily demonstrated by the accuracy of the constructed RSM model.

Zain et al. [13] integrated backpropagation neural network (BPNN) algorithm and GA to obtain a minimum surface roughness of the end-milled Ti6Al4V alloy taking into account the influence of cutting speed, feed rate, and depth of cut. The hybrid intelligent model reduced surface roughness to 0.139 µm at the optimized speed, feed rate, and rake angle (167.029 m/min, 0.025 mm/tooth, and 4.769°). The achieved roughness is quite lower than the corresponding values of experimental, BPNN, regression, and RSM with amounts reaching 26.8, 26.1, 25.7, and 49.8%, respectively. Similarly, the integrated BPNN-GA model has minimized the surface roughness and iteration as compared with the standard GA model to 0.61 and 23.9%, respectively.

AL-Khafaji [14] developed a radial basis network model based on the experimental data of turning AA7020-T6 alloy to estimate the chip thickness ratio as well as cutting forces. They found that these two responses are highly influenced by the input parameters. The optimum conditions were found using this model that maintains the chip thickness ratio and cutting forces at 1.21 and 240.46, respectively.

Moghri et al. [15] carried out a study in which they used both experiments and ANNs to establish a prediction model for the optimization of surface quality during the milling of polyamide-6 (PA-6) nanocomposites. The BPNN model was fed with spindle speed, feed, and content as inputs and surface roughness as output. GA was applied to train the BPNN due to the small data set provided by the full-factorial design. The findings recommended that feed rate and spindle speed have to be set on low and medium levels to generate the minimum surface roughness PA-6/NC specimen.

The neural network was adopted by Ibraheem [16] to predict the generated cutting forces during the machining of AISI 5210 alloy steel. The BPNN model was trained with 19 experimental runs consisting of input (speed, feed, depth of cut)-output (cutting forces) pairs. The developed model was tested with unseen six experimental data to check the model generalization. It was found that the produced cutting forces were significantly impacted by feed followed by the depth of cut and matching was achieved between the real and desired data.

The impact of end-milling variables on the machinability of high-strength carbon fibre composite material was investigated by Boga and Koroglu [17]. To estimate the attained surface roughness, a combined neural—genetic model was also developed. The analysis of the results revealed that the type of cutting tool and feed rate — whose optimal values were TiAlN-coated tool, 250 mm/rev beside 5,000 rev/min as cutting speed — had a significant impact on surface finish. Minimum mean square error (MSE) of 0.074 was attained using the hybrid model.

A machine learning algorithm and a physical-based method were combined by Rahimi *et al.* [18] to assess the chatter levels during the milling operation. The findings showed that the integrated model was able to predict the chatter with an accuracy reaching 98% and allowed for the deterministic physical-based model to implement additional training along the production phase.

Al-Zubaidi *et al.* [19] examined the performance of the gravitational search algorithm (GSA) during training the BPNN to predict the machining measure of Ti-6Al-4V end-milled surface by PVD-coated tool. The hybrid model was powerful in predicting the surface roughness of the machined surface with a very low MSE.

It can be noted from the above-cited works that they either mostly applied single neural network models (ANN) or trained the neural network with a single heuristic optimization algorithm to construct hybrid intelligent models



Figure 1: 5-axis DMU CNC milling machine.

such as GA–ANN, PSO–ANN, and GSA–ANN. Due to the important role of the machining processes in the manufacturing sector, it has become important to develop realistic and reliable intelligent models to predict the outcomes of this process. It is well known that machining is usually applied with impregnating cutting fluids and coolants, which negatively affect the environment, production cost, and human health. As world countries are struggling with the negative impact of climate change, they have steered their focus and attention toward sustainability and ecofriendly processing systems. Therefore, this study aimed to investigate the performance of the PSO–GSA hybrid algorithm during training the BPNN to predict the roughness of dry-end-milled surface of Ti6Al4V alloy with an uncoated cutting tool.

#### 2 Experimental work

A 5-axis CNC milling machine (Type DMU 70) was used to end-mill Ti6Al4V block. It is heavy-duty and high-performance machine where speed reaches 18,000 rpm and it has a fast transverse motion of 24 m/min. Figure 1 depicts the used machine. The titanium alloy being used in this research is considered hard to machine, and it is mainly used in aero-space and biomedical sectors. The mechanical properties of Ti6Al4V are illustrated in Table 1.

The end-milling process of titanium alloy was carried out in a dry condition using an uncoated cutting insert whose specifications are given in Table 2. The insert was fixed in the R217.69-1612.0-09-1A tool holder and has a diameter of 12 mm. The full-factorial design of the experiment with 27 orthogonal arrays was applied to generate 27 experimental runs and provide a statistical analysis of the achieved results. This array is also capable of presenting the interactions between the input factors and their influence on the output response. Three input parameters with three levels have been assigned, namely, cutting speed (50, 77.5, and 105 m/min), feed rate (0.1, 0.15, and 0.2 mm/tooth), and depth of cut (1, 1.5, and 2 mm). The radial depth of cut was set at 8 mm, and the surface roughness of the newly machined surface was measured triple times and averaged after each experiment. Table 3 provides the selected parameters and their levels in real and

Table 1: Ti6Al4V's mechanical properties

| Ultimate tensile strength, $\sigma_{\rm u}$ (MPa) | Yield strength, $\sigma_{\rm y}$ (MPa) | Young modulus, E (GPa) | Poisson's ratio (ν) | Hardness (HRC) |
|---|--|------------------------|---------------------|----------------|
| 950   | 880                                    | 113.8                  | 0.342               | 36             |

Table 2: Dimensions and specifications of the uncoated cutting insert

| Tool type                 | Insert<br>cutting<br>rake angle | Insert side<br>clearance<br>angle | Insert<br>helix<br>angle | Maximum<br>depth of<br>cut (mm) | Chamfer<br>width (mm) | r <sub>ε</sub> (mm) | Dimension 80° | s (mm) |            |
|---------------------------|---------------------------------|-----------------------------------|--------------------------|---------------------------------|-----------------------|---------------------|---------------|--------|------------|
|                           |                                 |                                   |                          |                                 |                       |                     | I             | d → Vε | 15° + + S+ |
| ISO grade<br>K20 uncoated | 24°                             | 11°                               | 15°                      | 5                               | 0.06 at 4°            | 0.8                 | 10            | 6      | 4          |

coded forms, while the experimental matrix is given in Table 4.

A 166 × 105 × 30 mm<sup>3</sup> block of Ti6Al4V alloy was prepared for the end-milling process by catching it firmly with a vice and pocket-machined to eliminate any contamination, rust, dust, or residual stresses. A G-code was written, and surface roughness (Ra) was measured by the MpiMahrperthometer roughness tester. Figure 2 displays the experimental setup.

### 3 Development of integrated neural network-evolutionary models

Machining processes are material removal operations in which some parameters contribute and interact to produce a desired response. This process is complex and involves high linearity that traditional models stand infirm to provide a good correlation between independent inputs and dependent outputs.

Here comes the role of AI techniques to fill up this gap and presents good mapping between input-output pairs. ANNs are among the most important AI algorithms that can

Table 3: Chosen end-milling parameters and corresponding levels

| Factors              | Unit       |     | Levels |     |
|----------------------|------------|-----|--------|-----|
|                      |            | 0   | 1      | 2   |
| A-Cutting speed      | (m/min)    | 50  | 77.5   | 105 |
| B-Feed rate          | (mm/tooth) | 0.1 | 0.15   | 0.2 |
| C-Axial depth of cut | (mm)       | 1   | 1.5    | 2   |

perform numerous tasks such as function approximation, classification, pattern recognition, and clustering. The BPNN is widely used by the researchers, although it experiences trapping in local solution and has a low convergence rate. Accordingly, this study aimed to integrate a BPNN with some evolutionary algorithms, namely, PSO and hybrid PSO-GSA.

Table 4: Experimental matrix of the 27th runs

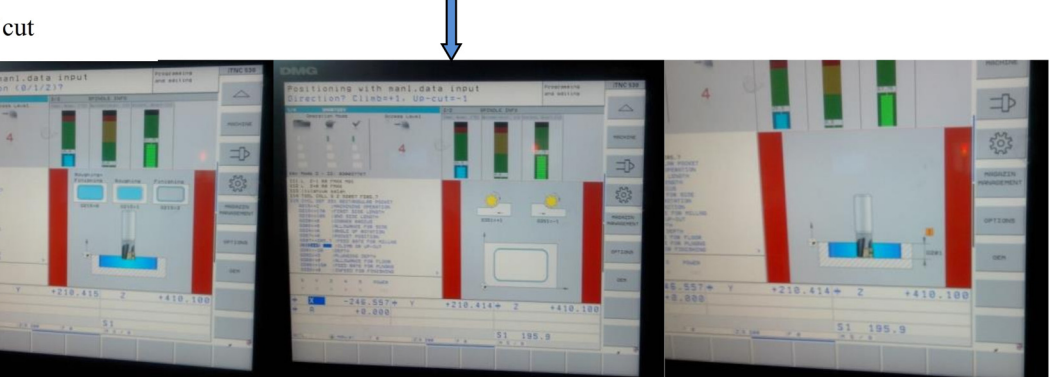
| Number | Cutting speed | Feed rate | Axial depth of cut |
|--------|---------------|-----------|--------------------|
| 1      | 50            | 0.1       | 1                  |
| 2      | 50            | 0.15      | 1.5                |
| 3      | 50            | 0.2       | 2                  |
| 4      | 77.5          | 0.1       | 1                  |
| 5      | 77.5          | 0.15      | 1.5                |
| 6      | 77.5          | 0.2       | 2                  |
| 7      | 105           | 0.1       | 1                  |
| 8      | 105           | 0.15      | 1.5                |
| 9      | 105           | 0.2       | 2                  |
| 10     | 50            | 0.1       | 1.5                |
| 11     | 50            | 0.15      | 2                  |
| 12     | 50            | 0.2       | 1                  |
| 13     | 77.5          | 0.1       | 1.5                |
| 14     | 77.5          | 0.15      | 2                  |
| 15     | 77.5          | 0.2       | 1                  |
| 16     | 105           | 0.1       | 1.5                |
| 17     | 105           | 0.15      | 2                  |
| 18     | 105           | 0.2       | 1                  |
| 19     | 50            | 0.1       | 2                  |
| 20     | 50            | 0.15      | 1                  |
| 21     | 50            | 0.2       | 1.5                |
| 22     | 77.5          | 0.1       | 2                  |
| 23     | 77.5          | 0.15      | 1                  |
| 24     | 77.5          | 0.2       | 1.5                |
| 25     | 105           | 0.1       | 2                  |
| 26     | 105           | 0.15      | 1                  |
| 27     | 105           | 0.2       | 1.5                |

A. Setting machine to zero set to start pocketing process



B. pocketing process to remove dust and contaminations

C.Selecting type of roughing and milling mode, setting up cutting speed, feed rate, axial and radial depth of cut



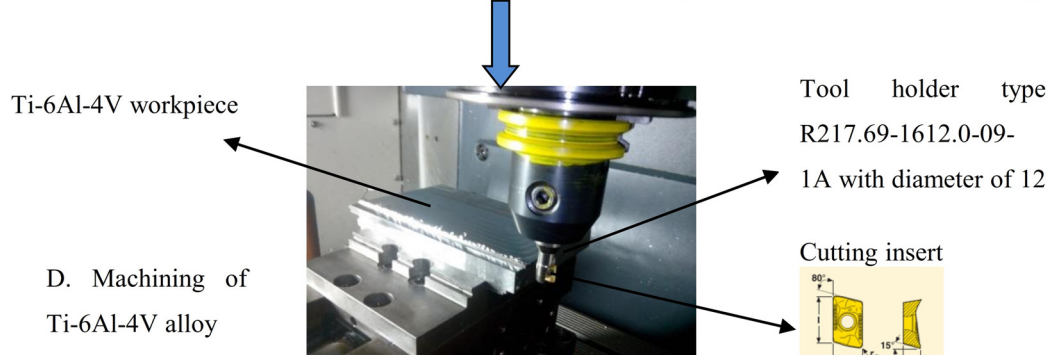


Figure 2: Experimental setup.

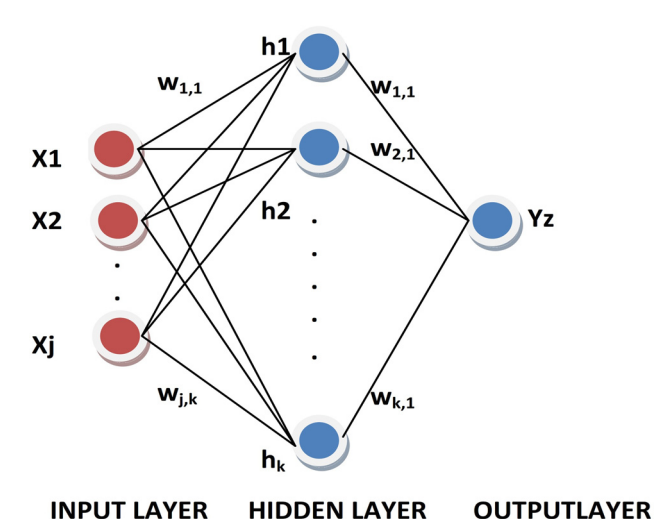


Figure 3: Feed-forward neural network with a single hidden layer.

Figure 3 shows a neural network with a multi-layer feedforward algorithm having a single hidden layer, and its training can be performed by implementing the following steps:

- Weight initialization
- · Feed-forward phase
- Error backpropagation
- Weight and bias adjustment

Concerning the first step, weights must be set to small and random values to avoid saturation. Each input neuron in the feed-forward gets input signal Xj and delivers it to the hidden ones. The hidden net is produced via summing of weighted input plus bias as given below:

$$hk = \sum_{j=1}^{J} Wj, k \times Xj + \text{bias}k.$$
 (1)

The aforementioned net proceeds to the activation function as illustrated in the following equation:

$$Hk = f(hk). (2)$$

Similarly, the output net is generated by summing the weighted hidden net plus its bias:

$$yz = \sum_{k=1}^{K} Wk, z \times Xk + \text{bias}z.$$
 (3)

In the same way, the activation function is applied to the output net in Eq. (3):

$$Yz = f(yz). (4)$$

The objective function (error function) is calculated using the following equation:

$$EF = \sum_{i=1}^{n} \frac{(d-Y)^2}{n}.$$
 (5)

The parameters of BPNN, for instance, number of hidden neurons, number of hidden layer, learning rate, momentum, and number of iterations were selected and set on: 1-20 hidden neurons, single hidden layer, 0.01, 0.9, and 500 iterations, respectively. The following subsections present a description of how this integration is accomplished to develop AI-integrated models to estimate the surface finish of the milled part with high accuracy. In general, the evolutionary algorithms need an objective function to optimize (either minimization or maximization of the last equation will be used by the evolutional techniques to extract the optimum combinations of weights and biases that ensure minimum error between the desired and real targets (Tzs)).

#### 3.1 Development of the integrated **BPNN-PSO** model

Eberhart and Kennedy invented the PSO algorithm. Its mechanism was inspired by the behaviour of social bird flocks [20]. PSO likens GA to the initialization of a population with random potential solutions and looking for the best solution. However, in PSO, there are no crossovers or mutations like in GA, where all the particles are traced through the search space of the optimum particle. During the swarm movement, the particles track two important fitness values (pbest and gbest). The particles concerned with the best fitness value are likened to a pacemaker, and each particle maintains tracking of its position coordinates in the search space. This fitness value is saved, where it is referred to as pbest. When a particle regards the entire population as its topological neighbours, the best pbest values is a global and called gbest.

The population of candidate solutions (particles) of the swarm is searching for the optimum solution during movement in the d-dimension search space. The fitness function is a quantitative measure of all particles. Each particle is characterized by velocity and position vectors (Vij and Pij). The velocity is updated to a new velocity by applying Eq. (6). Consequently, the new position can be calculated by summing up the previous position with a new velocity (Eq. (7)).

$$Vij(\text{new}) = w \times Vij(\text{previous}) + c1 \times \text{rand1}$$
  
  $\times (pbestij - pij) + c2 \times \text{rand2}$  (6)  
  $\times (gbestij - pij),$ 

$$Pij(new) = Pij(previous) + Vij(new),$$
 (7)

where w is the inertia weight and rand is a random number with [0,1] range. c1 and c2 are the positive constants, and they are set on 2. Generally, they are regarded as learning

Table 5: Parameters of the PSO algorithm

| No. | Parameters                | Value    |
|-----|---------------------------|----------|
| 1   | Population size           | 30       |
| 2   | Learning factors: c1 & c2 | 2        |
| 3   | Inertia weight            | 0.9, 0.5 |
| 4   | Maximum iterations        | 500      |

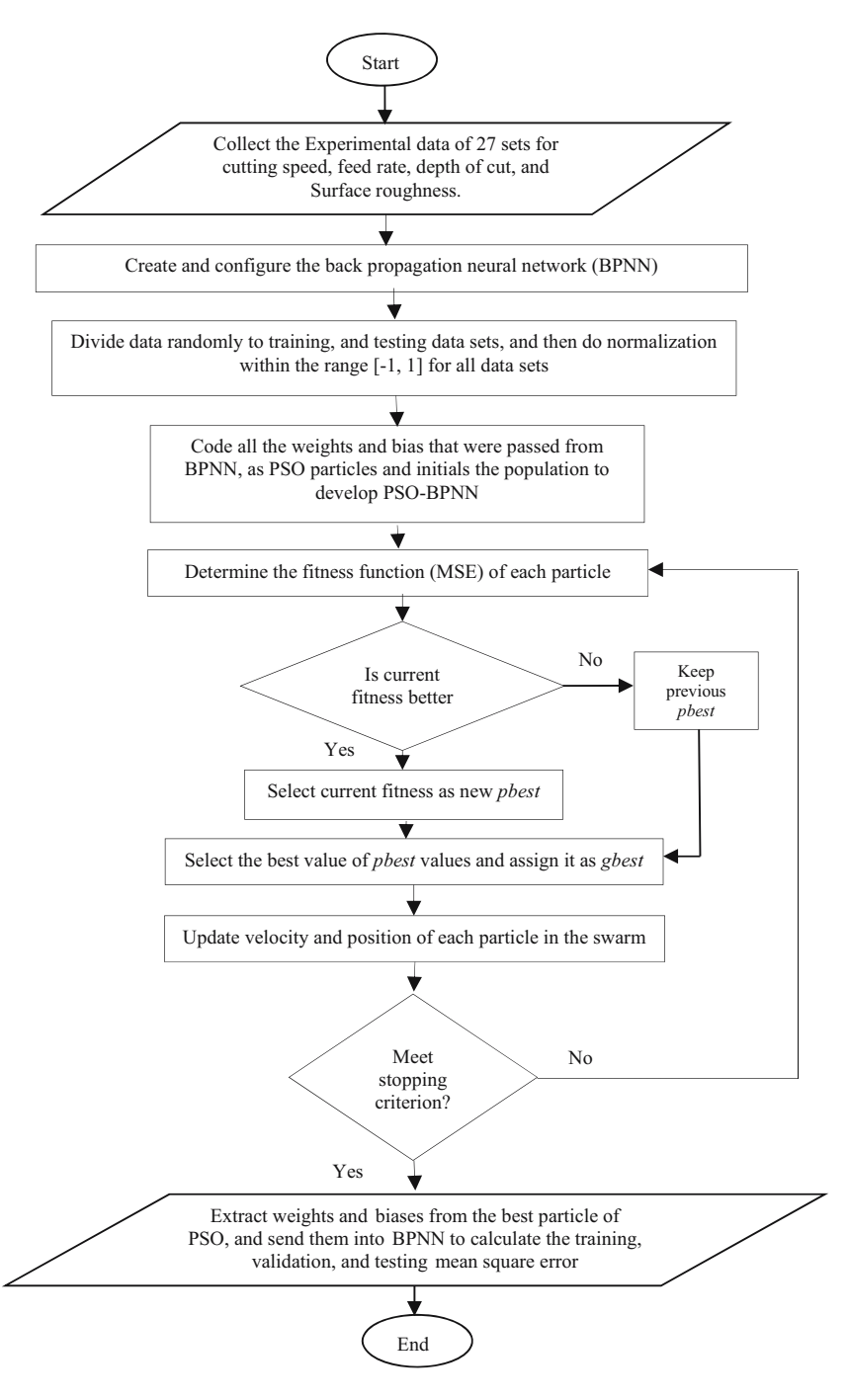


Figure 4: Flowchart of the integrated BPNN-PSO model.

factors. Table 5 shows the control parameters of the PSO algorithm. The c1 and c2 determine how far the swarm particles are from the global solution.

PSO optimization consists of several steps to accomplish the global solution (Figure 4):

- Population initialization (population size, particle velocities, positions, weights, and biases)
- The best fitness value in the current iteration is set as pbest and stored. The PSO is tracking another best value called gbest, which is so far the best value of Pbest particle in the swarm. These two values are important when implementing the PSO algorithm.
- Evaluate the fitness function of each particle in the swarm to recognize the pbest and gbest values.
- If the current fitness is less than the previous *pbest*, it is replaced with this current value for pbest. If not, the previous value remains as pbest.
- Select the best value of *pbest* values and assign it as a new *gbest*.
- Update the velocities and positions according to Eqs. (6) and (7), respectively.
- The updated swarm particles are flying again with their new positions (Eq. (7)).
- If the number of epochs has been reached, then stop the training, or else, repeat Steps 3–7.
- Extract weights and biases from the best particle of PSO, and send them into BPNN to calculate the MSE of training, validation, and testing for evaluation of the performance of BPNN-PSO models.

Minimization of the fitness function is the main target of the developed model to make the desired output of the model (predicted values) close to or near the Tzs.

#### 3.2 Development of the hybrid BPNN-PSO-GSA model

The PSO-GSA hybrid algorithm was developed by Mirjalili et al. [21]. To take advantage of the ability of each of them, the first (i.e., PSO) is distinguished by exploitation and the latter (i.e., GSA) is characterized by exploration. In other words, these hybrid algorithms combine the merits of both algorithms and exclude the demerits of them.

The equations of the gravitational search algorithm (GSA), which was developed by Rashedi et al. [22], were recalled here beside the hybrid PSO-GSA algorithm [21].

The positions of system agents (masses) are defined in Eq. (8), where ith agent in the dth space is positioned by  $x_i^d$ . By applying Newton's law, the attractive force  $F_{ij}^d(t)$  (Eq. (9)) between active and passive masses ( $M_{ai}$  and  $M_{vi}$ ) at Euclidian distance (Eq. (10)) is obtained.

$$Xi = (x_i^1, ..., x_i^d, ..., x_i^n)$$
 where  $i = 1, 2, 3, ..., N$ , (8)

$$F_{ij}^d(t) = G(t) \frac{M_{pi}(t) \times M_{aj}(t)}{R_{ij}(t) + \varepsilon} (x_j^d(t) - x_i^d(t)), \tag{9}$$

where gravitational, time, and minor constant were represented by G(t), t, and  $\varepsilon$ , respectively.

$$R_{ij}(t) = ||X_i(t), X_j(t)||^2$$
(10)

To give stochastic nature for  $F_{ii}^d(t)$ , a random weight is added to find out the total force (Eq. (11)) to calculate the dth acceleration at time t of ith agent:

$$F_i^d(t) = \sum_{j=1, j\neq i}^N \operatorname{rand}_j F_{ij}^d(t), \tag{11}$$

$$a_i^d(t) = \frac{F_i^d}{M_{ii}(t)},$$
 (12)

where the  $M_{ii}$  refers to the *i*th inertia.

To get a benefit for the exploitation capability of the PSO, Eqs. (6) and (7) are modified here to obtain the velocity and position of the new agent by incorporating the acceleration (Eq. (12)) into PSO-GSA as shown below:

$$Vij(\text{new}) = w \times Vij(\text{previous}) + c'1 \times r \quad \text{and} \quad 1^*aij$$
  
  $+ c'2^*r \quad \text{and} \quad 2 \times (gbestij - pij),$  (13)

$$Pij(\text{new}) = Pij(\text{previous}) + Vij(\text{new}).$$
 (14)

Initially, the gravitational constant is given an initial value  $(G_0)$  and it decreases with time to empower the accuracy of the search. Therefore, this constant is a function of  $(G_0)$  and time (t):

$$G = G(G_0, t). \tag{15}$$

The fitness equation is used to determine each of the gravitational and inertia masses. The heaviest mass represents the more efficient and attractive mass that moves at a slow speed. Equalizing the inertia and gravitational masses enables us to find out the masses using the fitness masses as given in Eqs. (16)-(18):

Table 6: Parameters of the PSO-GSA algorithm

| No. | PSO-GSA parameters        | Value    |
|-----|---------------------------|----------|
| 1   | Population size           | 30       |
| 2   | Gravitational constant    | 100      |
| 3   | Learning factors: c1 & c2 | 2        |
| 4   | Inertia weight            | 0.9, 0.5 |
| 5   | Maximum iterations        | 500      |

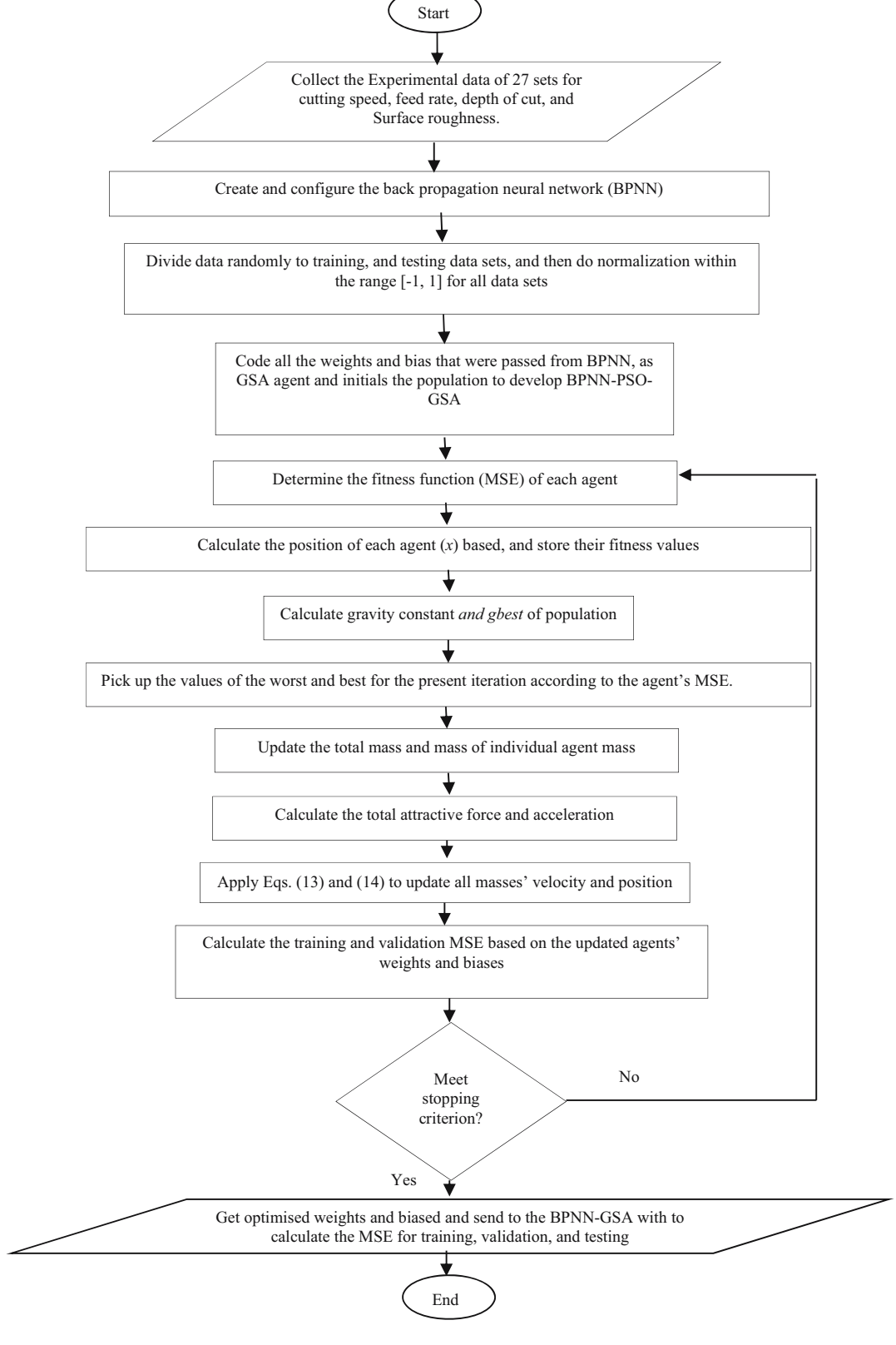


Figure 5: Flowchart of the integrated BPNN-PSO-GSA model.

$$M_{ai} = M_{pi} = M_{ii} = M_i i = 1, 2, 3, ..., N,$$
 (16)

$$m_i(t) = \frac{\text{fit}_i(t) - \text{worst}(t)}{\text{best}(t) - \text{worst}(t)},$$
(17)

$$M_i(t) = \frac{m_i(t)}{\sum_{i=1}^{N} m_i(t)},$$
(18)

where  $fit_i(t)$  refers to the *i*th fitness values at time *t*. For minimization problem as in the current study, the worst and best at time (t) are given in the following equations:

$$best(t) = maxfit_i(t), (19)$$

$$worst(t) = minfit_i(t).$$
 (20)

To develop BPNN-PSO-GSA, the following steps must be carried out:

- · Initialize the population represented by the sent weights and biases by the BPNN.
- Coding both of weight and bias in the position vector form.
- Calculate the position of each agent (x) based, and store their fitness values.
- Calculate the gravity and *g-best* of the population.
- · Pick up the values of the worst and best for the present iteration according to the MSE of the agent.
- Update the total mass and mass of individual agent mass.
- · Calculate the total attractive force and corresponding acceleration.
- Apply Eqs. (13) and (14) to update the velocity and position of all masses.
- Calculate the training and validation of MSE based on the weights and biases of updated agents.
- · If the stopping criterion is fulfilled, stop training and inject the BPNN-PSO with optimized weights and biases to calculate the MSE of training, validation, and testing. If not, repeat Steps 3-9.

The PSO-GSA parameters are given in Table 6, while Figure 5 illustrates the sequence steps for developing the integrated BPNN-PSO-GSA model.

#### 4 Results and discussion

#### 4.1 Analysis of surface roughness model

In this study, the full-factorial method was used as the design of experiment to generate an L27 orthogonal array to investigate the impact of each cutting condition and their interaction on the surface roughness of milled Ti6Al4V alloy with an uncoated tool under dry cutting conditions. Table 7

Table 7: Experimental data of the machined Ti6Al4V alloy

| Number           | Cutting<br>speed | Feed<br>rate | Depth<br>of cut | Surface<br>roughness (µm) |
|------------------|------------------|--------------|-----------------|---------------------------|
| 1                | 50               | 0.1          | 1               | 0.539                     |
| 2                | 50               | 0.15         | 1.5             | 0.882                     |
| 3                | 50               | 0.2          | 2               | 1.744                     |
| 4                | 77.5             | 0.1          | 1               | 0.548                     |
| 5                | 77.5             | 0.15         | 1.5             | 0.966                     |
| 6                | 77.5             | 0.2          | 2               | 1.644                     |
| 7                | 105              | 0.1          | 1               | 0.552                     |
| 8                | 105              | 0.15         | 1.5             | 0.918                     |
| 9                | 105              | 0.2          | 2               | 1.412                     |
| 10               | 50               | 0.1          | 1.5             | 0.8                       |
| 11               | 50               | 0.15         | 2               | 1.229                     |
| 12               | 50               | 0.2          | 1               | 1.201                     |
| 13               | 77.5             | 0.1          | 1.5             | 0.68                      |
| 14               | 77.5             | 0.15         | 2               | 1.156                     |
| 15               | 77.5             | 0.2          | 1               | 1.076                     |
| 16               | 105              | 0.1          | 1.5             | 0.585                     |
| 17               | 105              | 0.15         | 2               | 1.134                     |
| 18               | 105              | 0.2          | 1               | 1.043                     |
| 19               | 50               | 0.1          | 2               | 0.56                      |
| 20               | 50               | 0.15         | 1               | 1.130                     |
| 21               | 50               | 0.2          | 1.5             | 0.942                     |
| 22               | 77.5             | 0.1          | 2               | 0.714                     |
| 23               | 77.5             | 0.15         | 1               | 0.687                     |
| 24               | 77.5             | 0.2          | 1.5             | 1.104                     |
| 25               | 105              | 0.1          | 2               | 0.611                     |
| 26               | 105              | 0.15         | 1               | 0.562                     |
| 27               | 105              | 0.2          | 1.5             | 0.956                     |
| Minimum<br>value | 0.539            |              |                 |                           |
| Maximum<br>value | 1.744            |              |                 |                           |
| Average<br>value | 0.954            |              |                 |                           |

shows the surface roughness when end-milling Ti6Al4V alloy. As stated in the previous section, the surface roughness value of milled Ti6Al4V alloy represents the average of three measurements taken at the beginning, middle, and end of the milling pass. Subsequently, the significant parameters that influence the machining performance measure (surface roughness) were assigned using ANOVA. An ANOVA result for the surface roughness of the uncoated tool is shown in Table 8. In this work, the significance level of 0.05 is taken into consideration in the resulting analysis, because the main significant effect obtains an occurrence probability (P) that is equal to or less than 0.05.

When the effect of independent parameters is combined with its interaction with another independent parameter, a significant interaction has occurred. This combined effect results in a different response (surface roughness) when compared to the lack of interaction between

Table 8: ANOVA of surface roughness

| Source | Sum of squares | Degree of freedom | Mean square           | <i>F-</i> Value | Prob > F | Percent contribution (%) |
|--------|----------------|-------------------|-----------------------|-----------------|----------|--------------------------|
| Model  | 2.75           | 18                | 0.15                  | 8.59            | 0.0021   | _                        |
| Α      | 0.089          | 2                 | 0.045                 | 2.52            | 0.1417   | 3.099                    |
| В      | 1.71           | 2                 | 0.85                  | 48.1            | < 0.0001 | 59.16                    |
| C      | 0.52           | 2                 | 0.26                  | 14.69           | 0.0021   | 18.07                    |
| AB     | 0.031          | 4                 | $7.65 \times 10^{-3}$ | 0.43            | 0.7831   | 1.059                    |
| AC     | 0.048          | 4                 | 0.012                 | 0.68            | 0.6255   | 1.670                    |
| BC     | 0.35           | 4                 | 0.087                 | 4.88            | 0.0274   | 12.01                    |

parameters. The ANOVA and full-factorial method allow us to find the optimized cutting parameters that produce minimum surface roughness. Five diagnostic plots have been generated using this software, namely, normal probability plot of the residuals, residuals *versus* predicted values, outlier *versus* run order in addition to residuals *versus* run number, and predicted *versus* actual plots. Figure 6 shows those diagnostic plots depicting this model as possessing satisfactory goodness of fit *via* the normal distribution of data.

Referring to Table 8, it is obvious that this model is significant when its F value is 8.59. Each factor obtains a P-value lower than 0.05, meaning it is a significant factor. When this criterion is applied to Table 8, it can be concluded that both feed rate (B) and depth of cut (C) are the significant factors that affect surface roughness. In other words, any change in their values results in diverse effects on the machining performance. The "Prob > F" of the feed rate is <0.0001, while the depth of cut has a recorded value of 0.0021. Consequently, the interactive influence is also significant for the feed rate and depth of cut, because it was 0.0274 "Prob > F," which was also less than 0.05. Meanwhile, the cutting speed (A) is not a significant factor, because it obtained a "Prob > F" value of more than 0.05.

It can be seen that the contribution values of each cutting condition have been added to the ANOVA table (Table 8). The feed rate has contributed to 59.16%, which is regarded as a high percentage compared with the other parameters. Meanwhile, the contribution of the depth of cut is 18.07%, while the cutting speed is limited to 3.099. The contribution of each factor is inversely proportional to its "Prob > F" value, where feed rate, for example, contributed the highest percentage, hence achieving the lowest "Prob > F" value." "Adeq Precision" measures the signal-to-noise ratio, where a value that is greater than 4 is desirable. The ratio of 10.515 is indicative of an adequate signal, making this model useful for design space navigation.

## 4.2 Effects of cutting process parameters on surface roughness

In the previous section, the full-factorial model was statistically analysed using ANOVA. The analysis revealed both the significant and insignificant factors. In this section, the performance of the machining measure will be assessed, and the effect of cutting conditions on this machining measure will be investigated. To do this, it is necessary to study the combined impact of each two cutting conditions while keeping the third constant. Hence, the design of experiment software has provided interaction graphs for all cutting conditions. Each graph consisted of three plots, with three holding values for one of the cutting conditions. The model predicted points are represented by squares, rhomboids, and triangles, while the circular points refer to the design points. The black, red, and green colours are assigned to the low, medium, and high levels of the endmilling parameters for both design and predicted points. The predicted points are connected via dotted lines. The interactive graph depicted in Figure 7 shows how the surface roughness is impacted by the feed rate and cutting speed with a 1, 1.5, and 2 mm depth of cut.

With a 1 mm depth of cut, the surface roughness values decrease when the cutting speed increases for medium and high feed rate levels. For the low feed rate, there is a very slight change in surface roughness for all cutting speed levels. Design points 1, 4, and 7 recorded minimum surface roughness (0.53, 0.54, and 0.55  $\mu$ m), which is represented by low feed rate and depth of cut, accompanied by low, medium, and high cutting speeds. The dotted lines are moving up when increasing the feed rate along different cutting speeds, which is reflected in the highly significant effect of the feed rate. Moving to Figure 7b the same graph with a 1.5 mm depth of cut as the holding value, the behaviour became different. At medium and high feed rates, the change in surface roughness along different cutting speeds is like a ramp.

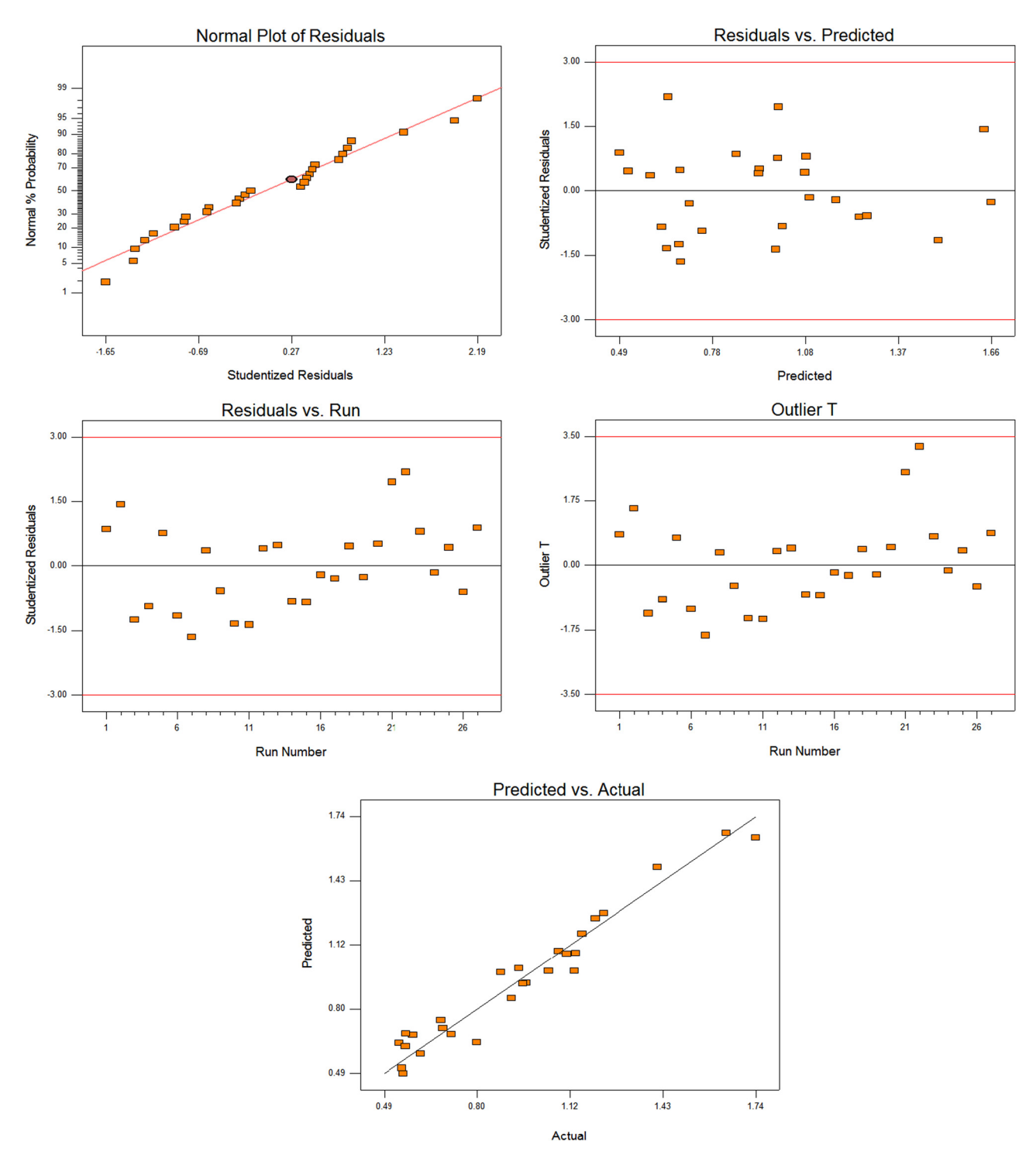
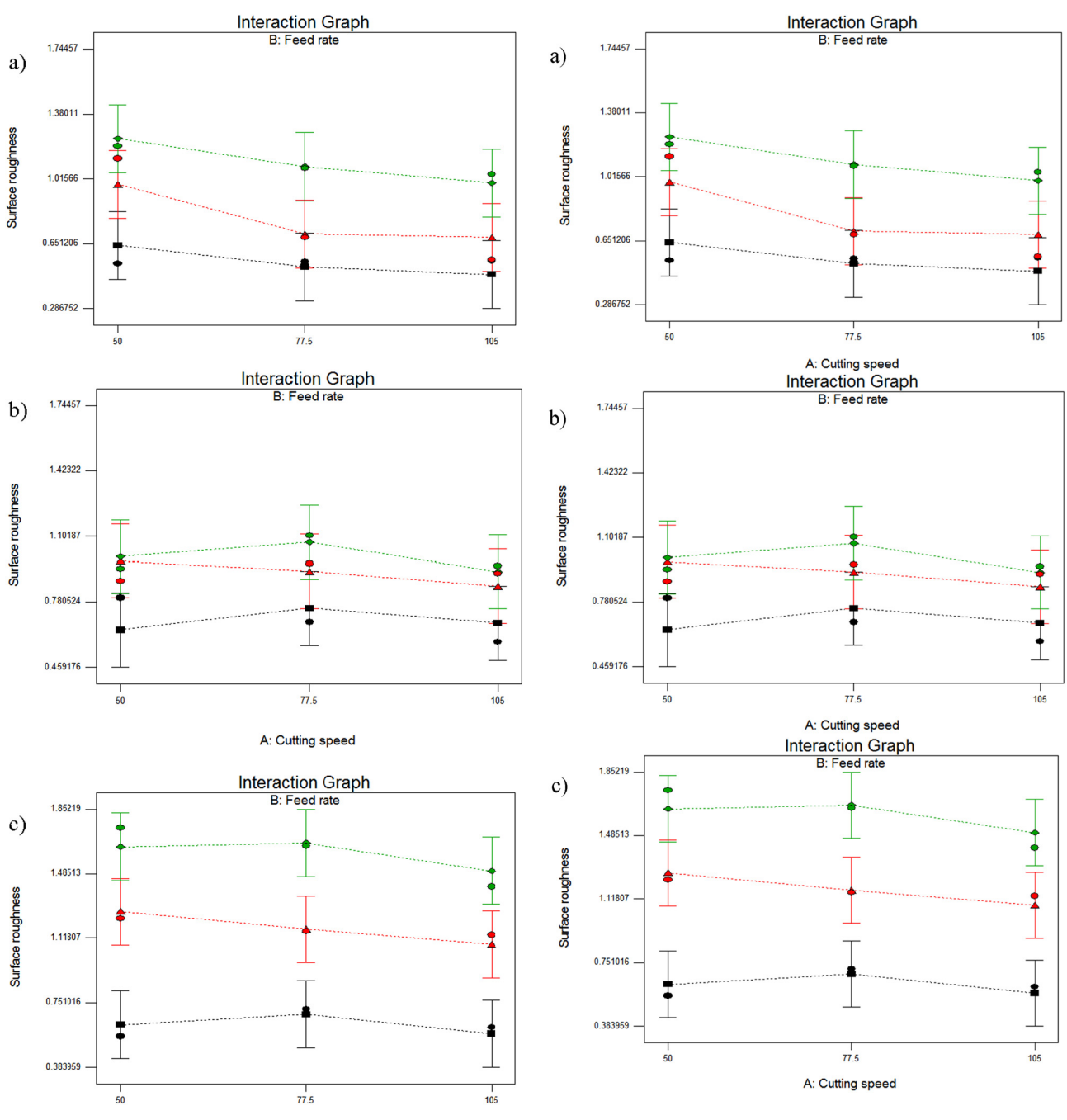


Figure 6: Residual model diagnostic for surface roughness.



**Figure 7:** Surface roughness interactive graph against cutting speed and feed rate with three holding values of depth of cut: (a) 1 mm, (b) 1.5 mm and (c) 2 mm.

A: Cutting speed

Meanwhile, the linear reduction in surface roughness with increasing cutting speed occurred. Hence, design point 16 resulted in the minimum surface roughness for this plot, at  $0.58\,\mu m$ . Also, the impact of feed rate is obvious when it is increased from low, through medium, to high levels.

**Figure 8:** Surface roughness interactive graph against cutting speed and depth of cut with three holding values of feed rate: (a) 0.1 mm/tooth, (b) 0.15 mm/tooth and (c) 0.2 mm/tooth.

Figure 7c reveals two important things. Firstly, the depth of cut can be set to a high level and accompanied by a high cutting speed and low feed rate to achieve acceptable surface roughness (design point 25). Secondly, the significant effect of feed rate is much clearer when it is combined with a high depth of cut compared with the first and second plots for the same plot. Hence, the high levels of

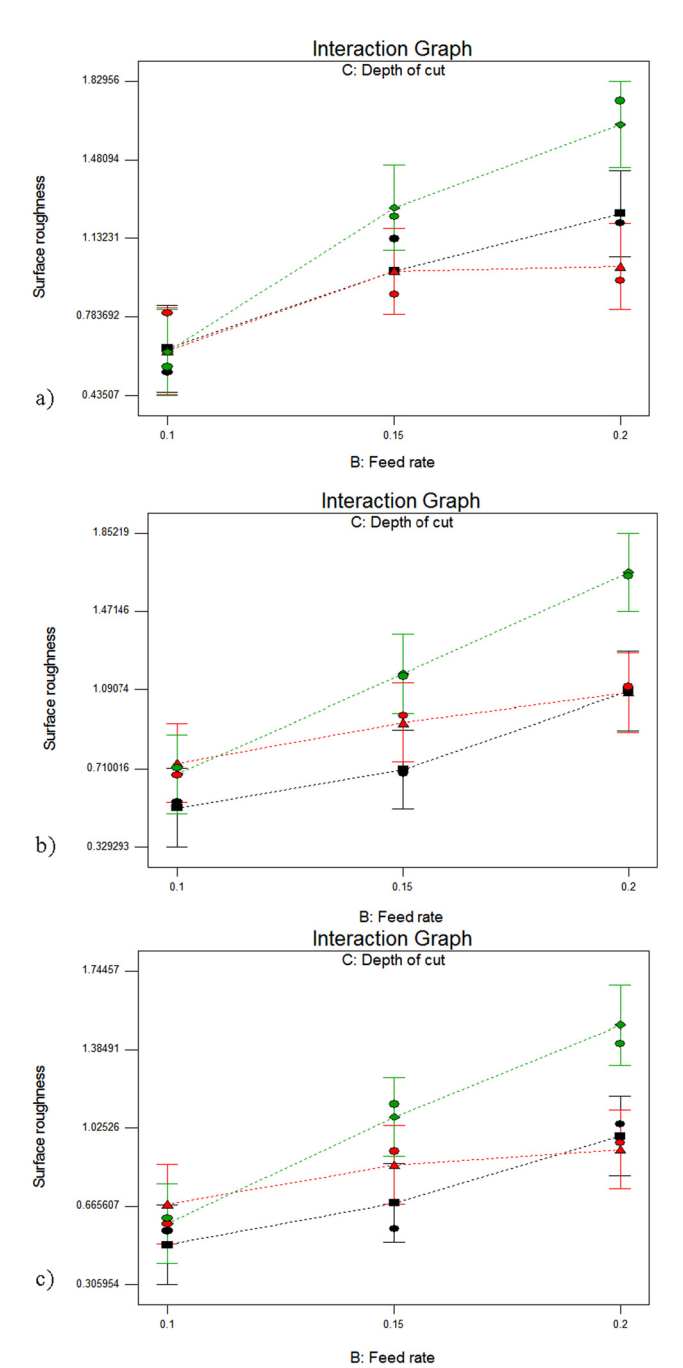


**Figure 9:** Surface roughness interactive graph against feed rate and depth of cut with three holding values of cutting speed: (a) 50 m/min., (b) 77.5 m/min., and (c) 105 m/min.

feed rate and depth of cut should be avoided to maintain an acceptable surface roughness value. The cutting speed in this context is not significant.

Figure 8 shows the surface roughness interactive graph vs cutting speed and depth of cut with three holding values for feed rate. Figure 8a reveals that with a low feed rate, it is possible to choose any combined settings of cutting speed and depth of cut, where the maximum surface roughness

does not exceed  $0.8 \, \mu m$  (design point 10), and the minimum is  $0.53 \, \mu m$  (design point 1).

The significant effect of feed rate was starting to express itself when its value increased to 0.15 and 0.2 mm/tooth (Figure 8b and c). The integrated influence of feed rate and depth of cut is significant. Numerically, design points 3, 6, and 9 reported the maximum surface roughness, with 1.7, 1.6, and 1.4  $\mu$ m, respectively. Those points are characterized by high feed rates and depth of cut with different cutting speed levels (Figure 8c). Meanwhile, Figure 8b registers the minimum roughness at 0.56  $\mu$ m, which originated from high cutting speed, medium feed rate, and low depth of cut (design point 26). Also, design point 23 achieved a good surface roughness of 0.68  $\mu$ m when using medium cutting speed and feed rate accompanied by low depth of cut. Only these two points should be taken into consideration as good surface roughness for this particular space.

Figure 9 represents the surface roughness interactive graph vs feed rate and depth of cut with three holding values of cutting speed. Cutting speed has no significant effect on the milled surface roughness. However, the significant effect of feed rate and depth of cut is shown in all three plots of the same figure. At any cutting speed, when the feed rate is integrated with a depth of cut at medium–medium or high–high levels, the produced surface roughness is higher than 0.8  $\mu$ m. On the contrary, at any cutting speed, all the design points that are located in the bottom-left corner of all three plots produced surface roughness of less than or equal to 0.8  $\mu$ m.

To sum up, the minimum surface roughness can be achieved at a low feed rate and depth of cut with any cutting speed within the specified range. Also, with medium cutting speed and low depth of cut, the feed rate can be set to a medium level to obtain good surface roughness. High cutting speeds, accompanied by high depth of cut, can maintain acceptable surface roughness to increase the metal removal rate and improve productivity, but the feed rate should be set at a low level. Moreover, the most important parameters that affect surface roughness significantly are the feed rate and depth of cut, but not to the same extent. The combined effect of both feed rate and depth of cut is also significant and affects the machining performance measure; therefore, they should be set at a low level. In general, a good surface finish can be achieved at high cutting speed accompanied by a low feed rate and depth of cut [23]. These results agreed with the ANOVA, which revealed that the most significant factors are feed rate (B), followed by depth of cut (C) and the combined effect of both (BC). On the other hand, both experimental results and statistical analysis of the ANOVA table showed, without a doubt, that the cutting speed and

Table 9: Optimum end-milling parameters

| Milling parameters and response | Target           | Lower limit | Higher limit | Optimum parameters |
|---------------------------------|------------------|-------------|--------------|--------------------|
| Cutting speed                   | Within the range | 50          | 105          | 105                |
| Feed rate                       | Within the range | 0.1         | 0.2          | 0.1                |
| Axial depth of cut              | Within the range | 1           | 2            | 1                  |
| Surface roughness               | Minimize         | 0.539       | 1.744        | 0.48               |



Figure 10: Optimum cutting conditions for surface roughness.

their interactions with feed rate and depth of cut are not significant. Hence, cutting speed can be set to any value within the range, although the preferred level is set to a high level for the aforementioned reasons.

#### 4.3 Optimization of surface roughness

In the previous section, the effect of cutting conditions on milled Ti-6Al-4V alloy was investigated during dry-end milling with an uncoated insert tool. The interaction graphs that have been plotted in the previous section showed the significant effect of cutting conditions by investigating the output response (surface roughness). Furthermore, the produced surface roughness results from the combined effect of these cutting conditions. Accordingly, these interaction graphs could not specify the exact optimized parameters that maintained the lowest surface roughness. Design expert software itself solves this issue by providing an optimal solution, which ensures minimum surface roughness.

The objective of the optimization is to achieve minimum surface roughness while keeping all cutting conditions within its range to generate multiple solutions, which are ranked based on minimum surface roughness and maximum desirability. By following this objective, the minimum surface roughness produced from the best solution was  $0.488 \, \mu m$ .

Table 9 shows the optimized conditions with minimum roughness, respectively. The optimum conditions are 105 m/min, 0.1 mm/tooth, and 1 mm. A confirmation test for these optimum cutting conditions was carried out, and 0.48  $\mu$ m was determined to be the minimum surface roughness. It can be noted that the optimum surface roughness is less than the experimental value, with similar cutting conditions. The optimum conditions are plotted in the ram form as shown in Figure 10, with one desirability line.

#### 4.4 Results of the hybrid BPNN-PSO model

Minimization of the fitness function is the main target of the developed model to make the desired output of the model (predicted values) close to or near the Tzs. The optimized weights and biases enable BPNN–PSO to achieve the minimum MSE. Table 10 shows the findings of the BPNN–PSO models. The results for the BPNN–PSO models revealed that 3–8–1 is the best network structure of BPNN–PSO. It consists of eight hidden neurons, respectively. While three stands for the input vectors for the neural model, and one refers to the output. The MSE values were  $2.42 \times 10^{-5}$ , as the best minimum MSE in testing. The minimum values for the other three statistical measures were 0.028725, 0.022096, and 0.016734, respectively.

Table 10: Results of the hybrid BPNN-PSO algorithm

| No. of neuron |                       | Mean                  |                       |                       | Median                |                       |                       | STDV                  |                       |                       | Best                  |                       |
|---------------|-----------------------|-----------------------|-----------------------|-----------------------|-----------------------|-----------------------|-----------------------|-----------------------|-----------------------|-----------------------|-----------------------|-----------------------|
|               | Training              | Validation            | Testing               |
| 1             | 0.029091              | 0.008393              | 0.038036              | 0.029671              | 0.008672              | 0.029852              | 0.005822              | 0.005172              | 0.028672              | 0.015984              | $4.98 \times 10^{-4}$ | 0.00279               |
| 2             | 0.016974              | 0.00339               | 0.038913              | 0.016648              | 0.002493              | 0.030228              | 0.005964              | 0.003235              | 0.030278              | 0.006085              | $5.89 \times 10^{-4}$ | 0.003181              |
| 3             | $1.24 \times 10^{-2}$ | $2.16 \times 10^{-3}$ | 0.043618              | 0.01086               | $1.76 \times 10^{-3}$ | 0.03417               | $5.17 \times 10^{-3}$ | $1.85 \times 10^{-3}$ | 0.037018              | $5.13 \times 10^{-3}$ | $9.99 \times 10^{-5}$ | $2.59 \times 10^{-3}$ |
| 4             | $1.53 \times 10^{-2}$ | $2.18 \times 10^{-3}$ | 0.032799              | $1.54 \times 10^{-2}$ | $1.43 \times 10^{-3}$ | $2.21 \times 10^{-2}$ | $6.02 \times 10^{-3}$ | $2.20 \times 10^{-3}$ | 0.032979              | $5.36 \times 10^{-3}$ | $9.41 \times 10^{-5}$ | $2.24 \times 10^{-3}$ |
| 5             | $1.03 \times 10^{-2}$ | $1.52 \times 10^{-3}$ | $3.94 \times 10^{-2}$ | $9.94 \times 10^{-3}$ | $7.88 \times 10^{-4}$ | $3.74 \times 10^{-2}$ | $5.30 \times 10^{-3}$ | $1.98 \times 10^{-3}$ | 0.02511               | $1.18 \times 10^{-3}$ | $1.17 \times 10^{-4}$ | $4.64 \times 10^{-3}$ |
| 9             | $1.27 \times 10^{-2}$ | $1.94 \times 10^{-3}$ | 0.03456               | $1.20 \times 10^{-2}$ | $1.12 \times 10^{-3}$ | $2.46 \times 10^{-2}$ | $5.18 \times 10^{-3}$ | $2.20 \times 10^{-3}$ | 0.027757              | $2.54 \times 10^{-3}$ | $1.89 \times 10^{-4}$ | 0.004026              |
| 7             | $1.27 \times 10^{-2}$ | $1.94 \times 10^{-3}$ | 0.03456               | $1.20 \times 10^{-2}$ | $1.12 \times 10^{-3}$ | $2.46 \times 10^{-2}$ | $5.18 \times 10^{-3}$ | $2.20 \times 10^{-3}$ | 0.027757              | $2.54 \times 10^{-3}$ | $1.89 \times 10^{-4}$ | $4.03 \times 10^{-3}$ |
| 8             | $9.39 \times 10^{-3}$ | $9.46 \times 10^{-4}$ | $5.99 \times 10^{-2}$ | $8.30 \times 10^{-3}$ | $8.71 \times 10^{-4}$ | $3.64 \times 10^{-2}$ | $4.71 \times 10^{-3}$ | $5.72 \times 10^{-4}$ | $6.84 \times 10^{-2}$ | $3.14 \times 10^{-3}$ | $2.63 \times 10^{-4}$ | $2.42 \times 10^{-5}$ |
| 6             | $1.08 \times 10^{-2}$ | $1.16 \times 10^{-3}$ | 0.043423              | $9.91 \times 10^{-3}$ | $7.67 \times 10^{-4}$ | 0.033566              | $4.33 \times 10^{-3}$ | $1.06 \times 10^{-3}$ | $3.75 \times 10^{-2}$ | 0.004142              | $6.13 \times 10^{-5}$ | $3.39 \times 10^{-3}$ |
| 10            | $1.12 \times 10^{-2}$ | $1.85 \times 10^{-3}$ | 0.046969              | $1.19 \times 10^{-2}$ | $1.48 \times 10^{-3}$ | $3.53 \times 10^{-2}$ | $4.63 \times 10^{-3}$ | $1.76 \times 10^{-3}$ | 0.03605               | $5.19 \times 10^{-4}$ | $1.69 \times 10^{-4}$ | $2.16 \times 10^{-3}$ |
| 11            | $1.04 \times 10^{-2}$ | $1.23 \times 10^{-3}$ | 0.028725              | $9.43 \times 10^{-3}$ | $9.44 \times 10^{-4}$ | $2.70 \times 10^{-2}$ | $5.66 \times 10^{-3}$ | $1.08 \times 10^{-3}$ | 0.016734              | $1.08 \times 10^{-3}$ | $2.53 \times 10^{-5}$ | $1.82 \times 10^{-4}$ |
| 12            | $1.14 \times 10^{-2}$ | $1.18 \times 10^{-3}$ | 0.043005              | $1.06 \times 10^{-2}$ | $7.94 \times 10^{-4}$ | $4.58 \times 10^{-2}$ | $5.56 \times 10^{-3}$ | $1.80 \times 10^{-3}$ | 0.027089              | $8.86 \times 10^{-4}$ | $3.49 \times 10^{-5}$ | $2.84 \times 10^{-3}$ |
| 13            | $1.09 \times 10^{-2}$ | $1.37 \times 10^{-3}$ | 0.041399              | $1.04 \times 10^{-2}$ | $8.66 \times 10^{-4}$ | $3.59 \times 10^{-2}$ | $4.90 \times 10^{-3}$ | $1.21 \times 10^{-3}$ | $3.09 \times 10^{-2}$ | 0.003299              | $2.62 \times 10^{-4}$ | 0.00479               |
| 14            | $8.55 \times 10^{-3}$ | $2.06 \times 10^{-3}$ | 0.039243              | $7.65 \times 10^{-3}$ | $9.31 \times 10^{-4}$ | $3.88 \times 10^{-2}$ | $4.52 \times 10^{-3}$ | 0.002573              | 0.027477              | $1.07 \times 10^{-3}$ | $9.04 \times 10^{-5}$ | $3.15 \times 10^{-3}$ |
| 15            | $1.19 \times 10^{-2}$ | $1.30 \times 10^{-3}$ | 0.04153               | $1.12 \times 10^{-2}$ | $1.07 \times 10^{-3}$ | $3.34 \times 10^{-2}$ | $4.46 \times 10^{-3}$ | $7.75 \times 10^{-4}$ | 0.03024               | $3.92 \times 10^{-3}$ | $3.21 \times 10^{-4}$ | $4.01 \times 10^{-3}$ |
| 16            | $1.10 \times 10^{-2}$ | $1.27 \times 10^{-3}$ | 0.041029              | $9.40 \times 10^{-3}$ | $1.04 \times 10^{-3}$ | $3.37 \times 10^{-2}$ | $4.45 \times 10^{-3}$ | $1.21 \times 10^{-3}$ | 0.031436              | $4.54 \times 10^{-3}$ | $2.34 \times 10^{-5}$ | $9.52 \times 10^{-4}$ |
| 17            | $1.04 \times 10^{-2}$ | $7.79 \times 10^{-4}$ | 0.046612              | $1.01 \times 10^{-2}$ | $5.19 \times 10^{-4}$ | $4.28 \times 10^{-2}$ | $3.47 \times 10^{-3}$ | $8.02 \times 10^{-4}$ | $3.59 \times 10^{-2}$ | $5.39 \times 10^{-3}$ | $4.84 \times 10^{-5}$ | $5.37 \times 10^{-3}$ |
| 18            | $1.08 \times 10^{-2}$ | $9.30 \times 10^{-4}$ | 0.044737              | $1.08 \times 10^{-2}$ | $7.55 \times 10^{-4}$ | $3.93 \times 10^{-2}$ | $4.38 \times 10^{-3}$ | $1.04 \times 10^{-3}$ | 0.025988              | $3.53 \times 10^{-3}$ | $4.05 \times 10^{-5}$ | $8.87 \times 10^{-3}$ |
| 19            | $9.11 \times 10^{-3}$ | $8.29 \times 10^{-4}$ | 0.064196              | $8.95 \times 10^{-3}$ | $8.11 \times 10^{-4}$ | $5.52 \times 10^{-2}$ | $3.66 \times 10^{-3}$ | $4.07 \times 10^{-4}$ | 0.054012              | $3.78 \times 10^{-3}$ | $2.03 \times 10^{-4}$ | $1.03 \times 10^{-2}$ |
| 20            | $8.20 \times 10^{-3}$ | $6.80 \times 10^{-4}$ | 0.075661              | $7.51 \times 10^{-3}$ | $5.60 \times 10^{-4}$ | $5.61 \times 10^{-2}$ | $3.35 \times 10^{-3}$ | $6.02 \times 10^{-4}$ | 0.06773               | $3.35 \times 10^{-3}$ | $3.22 \times 10^{-5}$ | $8.10 \times 10^{-3}$ |
| Minimum       | 0.008204              | 0.00068               | 0.028725              | 0.007511              | 0.000519              | 0.022096              | 0.003354              | 0.000407              | 0.016734              | 0.000519              | $2.34 \times 10^{-5}$ | $2.42 \times 10^{-5}$ |

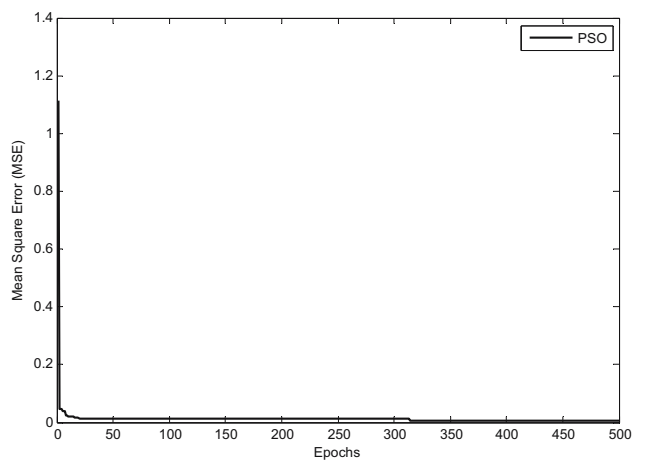
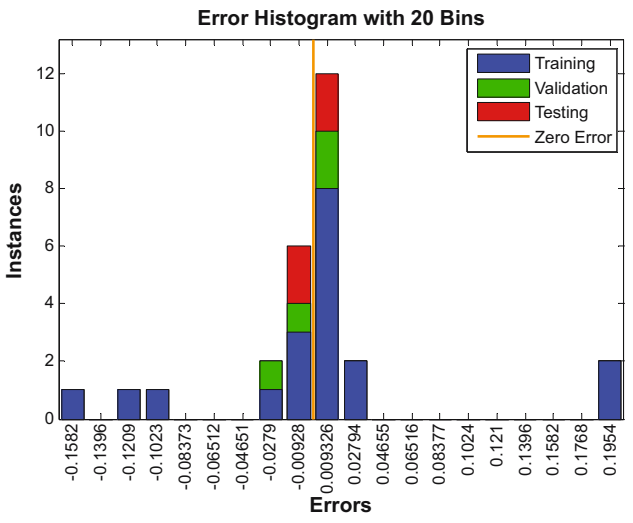


Figure 11: MSE vs epochs of the 3-8-1 BPNN-PSO best model.



**Figure 12:** Training, validation, and testing error histogram for the 3–8–1 BPNN–PSO model.

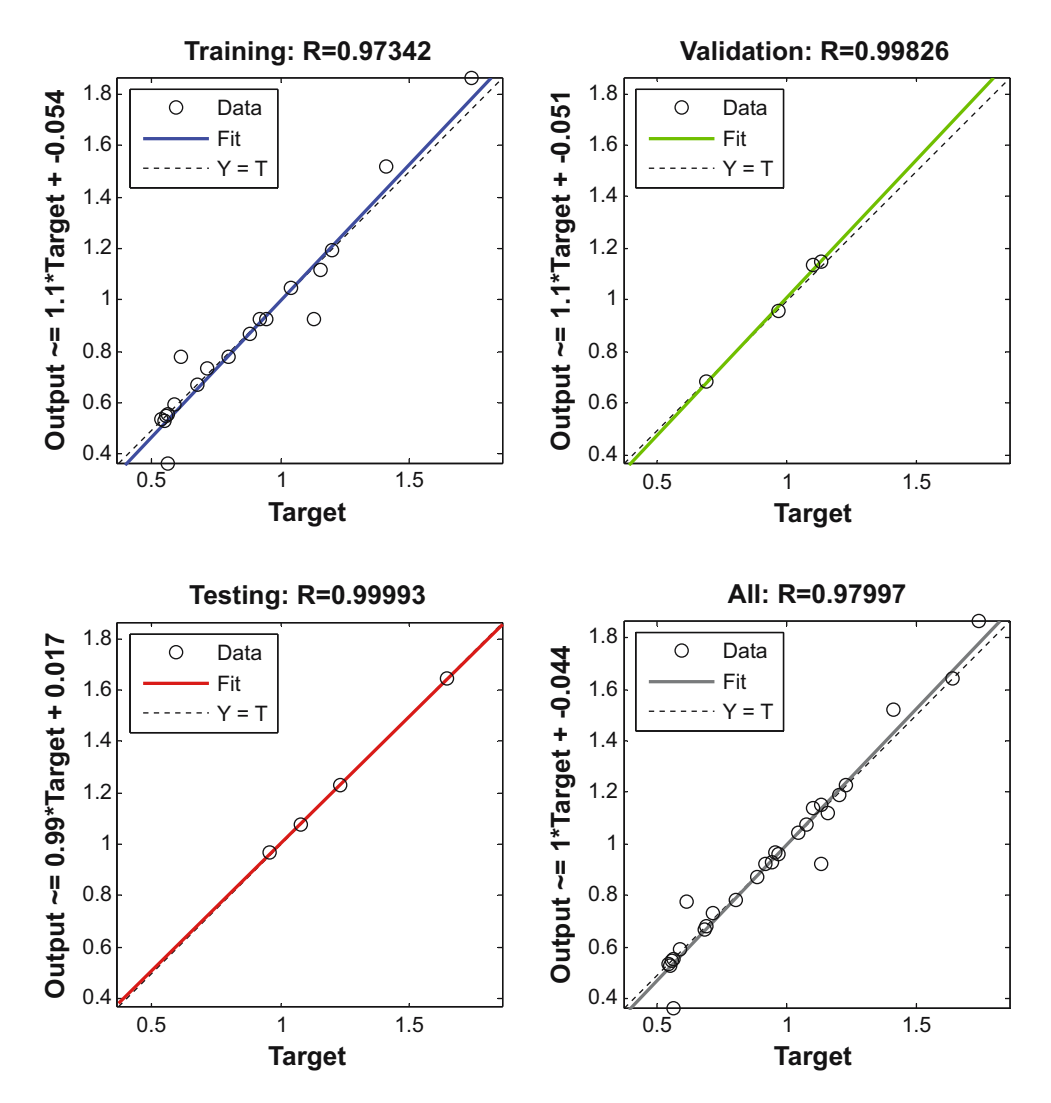


Figure 13: Training, validation, testing, and all regression plots for the 3-8-1 BPNN-PSO model.

Table 11: Results of the hybrid BPNN-PSO-GSA

|               |                       |                       |                       |          | :                     |                       |                       |                       |                       |                       |                       |                        |
|---------------|-----------------------|-----------------------|-----------------------|----------|-----------------------|-----------------------|-----------------------|-----------------------|-----------------------|-----------------------|-----------------------|------------------------|
| No. of neuron |                       | Mean                  |                       |          | Median                |                       |                       | SIDV                  |                       |                       | Best                  |                        |
|               | Training              | Validation            | Testing               | Training | Validation            | Testing               | Training              | Validation            | Testing               | Training              | Validation            | Testing                |
| I             | 0.02805               | 0.00841915            | 0.00328               | 0.027323 | 0.00519               | 0.026754              | 0.007418              | 0.008198              | 0.02626               | 0.001514              | $8.43 \times 10^{-5}$ | 0.000283               |
| 2             | 0.01769               | 0.0041765             | 0.06091               | 0.018153 | 0.00201               | 0.053475              | 0.009276              | 0.00568               | 0.0429                | 0.000541              | 0.000101              | 0.000736               |
| 3             | 0.01471               | 0.00274518            | 0.04779               | 0.013439 | 0.002452              | 0.038052              | 0.008505              | 0.002203              | 0.03799               | 0.000345              | $4.14 \times 10^{-5}$ | 0.000277               |
| 4             | 0.01093               | 0.00161028            | 0.05051               | 0.009306 | 0.001131              | 0.034873              | 0.00737               | 0.002046              | 0.0698                | 0.000297              | $8.56 \times 10^{-7}$ | $9.06 \times 10^{-5}$  |
| 2             | 0.00963               | 0.00186011            | 0.03739               | 0.008551 | 0.001071              | 0.031494              | 0.006569              | 0.002019              | 0.02801               | 0.00011               | $3.32 \times 10^{-5}$ | 0.000461               |
| 9             | 0.00853               | 0.00140709            | 0.05224               | 0.007909 | $7.84 \times 10^{-4}$ | 0.038457              | 0.006893              | 0.001821              | 0.04628               | $1.65 \times 10^{-5}$ | $3.19 \times 10^{-6}$ | 0.000887               |
| 7             | 0.00702               | $6.19 \times 10^{-4}$ | $6.04 \times 10^{-2}$ | 0.00497  | $3.65 \times 10^{-4}$ | 0.04904               | 0.005396              | $6.85 \times 10^{-4}$ | 0.03245               | $1.68 \times 10^{-5}$ | $7.86 \times 10^{-7}$ | 0.000216               |
| 8             | 0.00718               | $6.06 \times 10^{-4}$ | 0.06872               | 0.005566 | $4.29 \times 10^{-4}$ | 0.055746              | 0.006126              | $5.86 \times 10^{-4}$ | 0.05107               | 0.000113              | $3.71 \times 10^{-6}$ | 0.000747               |
| 6             | 0.00474               | $4.28 \times 10^{-4}$ | 0.04631               | 0.004407 | $2.17 \times 10^{-4}$ | $4.24 \times 10^{-2}$ | 0.0032                | $4.95 \times 10^{-4}$ | 0.02788               | $8.26 \times 10^{-6}$ | $1.95 \times 10^{-7}$ | 0.000171               |
| 10            | 0.00559               | $4.58 \times 10^{-4}$ | $6.33 \times 10^{-2}$ | 0.004441 | $2.41 \times 10^{-4}$ | 0.048054              | 0.004086              | $6.99 \times 10^{-4}$ | $5.65 \times 10^{-2}$ | $2.52 \times 10^{-5}$ | $8.54 \times 10^{-7}$ | 0.000907               |
| II            | 0.00305               | $1.30 \times 10^{-4}$ | $6.73 \times 10^{-2}$ | 0.002323 | $9.47 \times 10^{-5}$ | 0.051874              | 0.002745              | $1.52 \times 10^{-4}$ | 0.0479                | $3.44 \times 10^{-4}$ | $8.04 \times 10^{-7}$ | 0.001513               |
| 12            | 0.00476               | $2.44 \times 10^{-4}$ | 0.07945               | 0.003232 | $1.11 \times 10^{-4}$ | 0.058731              | 0.004027              | $3.30 \times 10^{-4}$ | 0.06357               | $4.49 \times 10^{-5}$ | $2.90 \times 10^{-6}$ | 0.002729               |
| 13            | 0.00334               | $1.94 \times 10^{-4}$ | 0.114                 | 0.002572 | $1.02 \times 10^{-4}$ | 0.081437              | 0.002906              | $2.27 \times 10^{-4}$ | 0.08894               | $1.17 \times 10^{-5}$ | $1.84 \times 10^{-7}$ | 0.000976               |
| 14            | 0.00411               | $3.76 \times 10^{-4}$ | 0.08472               | 0.003345 | $1.17 \times 10^{-4}$ | 0.088953              | 0.004134              | $5.99 \times 10^{-4}$ | $5.77 \times 10^{-2}$ | $3.75 \times 10^{-5}$ | $2.63 \times 10^{-7}$ | 0.000654               |
| 15            | 0.00362               | $3.20 \times 10^{-4}$ | 0.09173               | 0.002873 | $1.90 \times 10^{-4}$ | 0.057943              | 0.00268               | $3.98 \times 10^{-4}$ | $9.25 \times 10^{-2}$ | $6.00 \times 10^{-5}$ | $5.52 \times 10^{-7}$ | 0.000455               |
| 16            | 0.00213               | $1.59 \times 10^{-4}$ | 0.14279               | 0.001368 | $6.74 \times 10^{-5}$ | 0.127193              | 0.002423              | $2.31 \times 10^{-4}$ | 0.011995              | $2.13 \times 10^{-5}$ | $4.36 \times 10^{-7}$ | 0.001457               |
| 17            | 0.00365               | $1.13 \times 10^{-4}$ | 0.13705               | 0.003246 | $6.08 \times 10^{-5}$ | $6.43 \times 10^{-2}$ | 0.003545              | $1.21 \times 10^{-4}$ | 0.013689              | $9.67 \times 10^{-6}$ | $3.43 \times 10^{-7}$ | 0.00028                |
| 1 8           | 0.00217               | $8.43 \times 10^{-4}$ | 0.40358               | 0.001596 | $6.13 \times 10^{-5}$ | 0.107956              | 0.001654              | 0.003363              | $1.00 \times 10^{-2}$ | $1.18 \times 10^{-7}$ | $2.95 \times 10^{-9}$ | $3.78 \times 10^{-11}$ |
| 19            | 0.00129               | $3.31 \times 10^{-5}$ | 0.10529               | 0.001285 | $3.31 \times 10^{-5}$ | 0.105292              | 0.002184              | $8.71 \times 10^{-5}$ | 0.028723              | 0.002351              | $7.35 \times 10^{-5}$ | 0.0238928              |
| 20            | 0.00292               | $9.49 \times 10^{-5}$ | 0.19596               | 0.002304 | $6.13 \times 10^{-5}$ | 0.14165               | 0.003659              | $7.22 \times 10^{-5}$ | $7.57 \times 10^{-2}$ | $1.82 \times 10^{-4}$ | $4.88 \times 10^{-6}$ | 0.012984               |
| Minimum       | $1.29 \times 10^{-3}$ | $3.31 \times 10^{-5}$ | $3.28 \times 10^{-3}$ | 0.001285 | $3.31 \times 10^{-5}$ | $2.68 \times 10^{-2}$ | $1.65 \times 10^{-3}$ | $7.22 \times 10^{-5}$ | 0.02626               | $1.18 \times 10^{-7}$ | $2.95 \times 10^{-9}$ | $3.8 \times 10^{-11}$  |

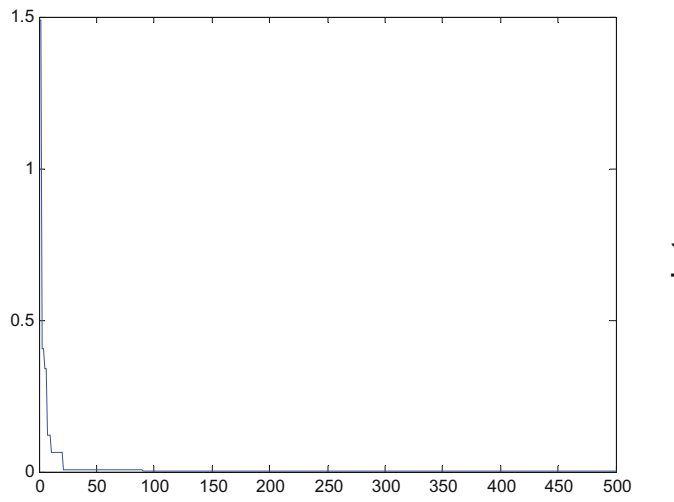
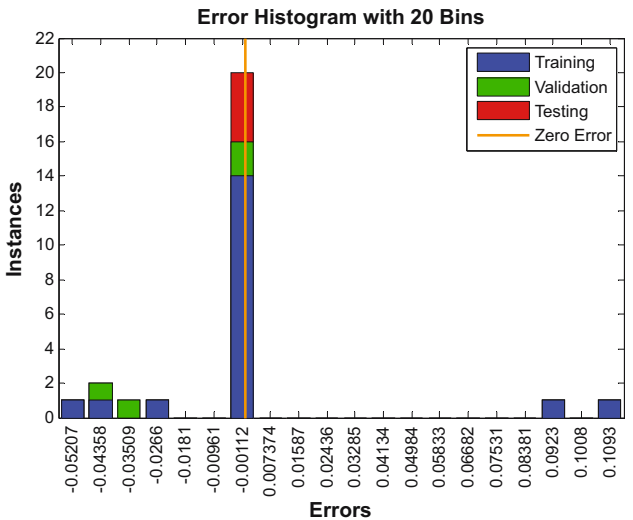


Figure 14: MSE vs epochs of the 3-18-1 BPNN-PSO-GSA best model.



**Figure 15:** Training, validation, and testing error histogram for the 3–18–1 BPNN–PSO–GSA model.

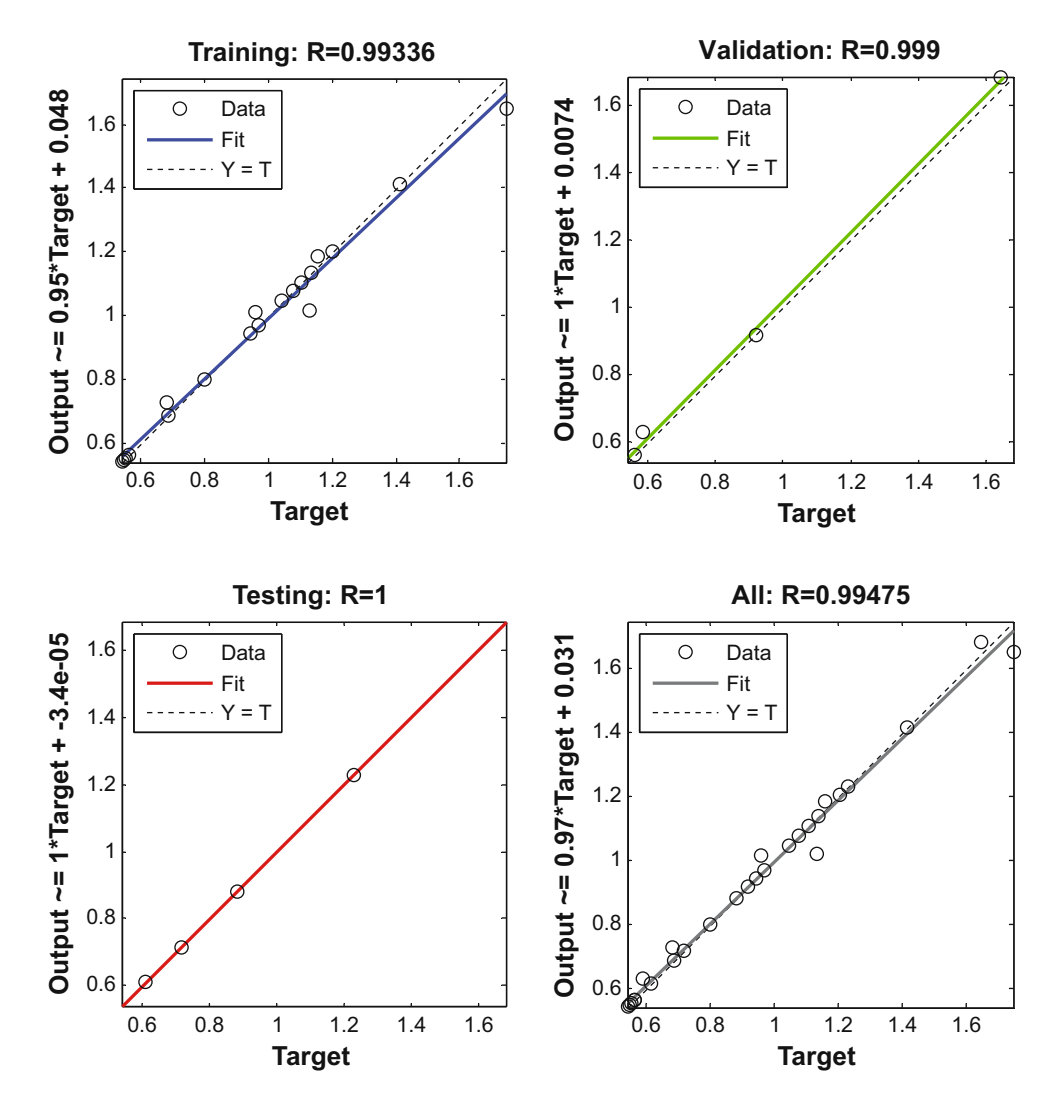


Figure 16: Training, validation, testing, and all regression plots for the 3-18-1 BPNN-PSO-GSA model.

Figure 11 shows the MSE of training versus epochs. It reveals a decrease in MSE with the elapsed epochs until approaching the minimum value. The trend of this figure takes an L-shape. This means that the improvement done by PSO iteration-by-iteration was done steeply in the first little iteration.

The error histogram was constructed based on the difference between the real and desired output for BPNN-PSO, as shown in Figure 12. The testing error range of the BPNN-PSO best model was -0.00928-0.00936. The red bar refers to the testing error and is closest to the bars of the zero line. As a result of this, BPNN-PSO achieved a high Rvalue, as will be seen later in the regression plot.

Regression plots in Figure 13 show the degree of matching between desired and real outputs in training, validation, and testing, respectively. It can be noted that all the training, validation, and testing data points are located on the best-fit lines, which are represented by blue, green, red, and grey, respectively. The BPNN-PSO algorithm achieved a testing R-value of greater than 0.99.

#### 4.5 Development of the integrated **BPNN-PSO-GSA** models

As stated in Section 3.2, the GSA was hybridized with PSO by Mirjalili et al. [21]. The BPNN has been trained by the hybrid PSO-GSA model to investigate its capability in modelling a complex and non-linear problem-like machining process as in the current study. Table 11 illustrates the four statistical measures for training, validation, and testing of BPNN-PSO-GSA models. It is clear the good performance of the hybrid model as BPNN-GSA did. Eighteen hidden neurons were sufficient to give the best MSE performance of  $3.8 \times 10^{-11}$  for the 3–18–1 structure.

Table 11 reveals the stable performance of the BPNN-PSO-GSA hybrid models at different hidden neurons in terms of the four statistical measures. It pointed out the significant role played by the hybridizing of GSA with PSO to maintain stable behaviour for different network structures. In other words, BPNN has gotten beneficiary to achieve more minimization for error function to make close matching between desired and target outputs. The 3-4-1 structure also had good performance with low MSE.

The mean, median, and best testing MSE of BPNN-PSO-GSA was lower than the corresponding values of the minimum MSE of BPNN-PSO. The exception was only the slightly larger standard deviation. The minimum MSE of

the developed hybrid model for the mean, median, standard deviation, and the best were  $3.28 \times 10^{-3}$ ,  $2.68 \times 10^{-2}$ , 0.02626, and  $3.8 \times 10^{-11}$ , respectively. Similarly, the trend of training MSE vs iteration was L-shaped as depicted in Figure 14. There was a fast drop for the MSE in the first few epochs to approach the global solution that is represented by the optimum set of weights and biases for the best network structure of 3-18-3. Then, the MSE takes right stable line until stopping criteria has been reached. The error histogram was constructed for blue training, green validation, and red testing as seen in Figure 15. Most of the training, validation, and testing errors are located around and near the zero line, which reflects the reliability of PSO-GSA's crucial role in training BPNN. To present a clear view regarding the BPNN-PSO-GSA model, the regression plots are presented in Figure 16. The excellent correlation between desired and Tzs is clearly illustrated by recording high R-values in the three phases, which were close to or equal to 1. Therefore, the capability of the hybrid PSO-GSA model in training BPNN with good reliability was approved by reaching minimum testing MSE (Table 11), low histogram errors (Figure 15), and excellent matching between desired and Tzs (Figure 16).

When the two best hybrid models (3-8-1 and 3-18-1) are placed in a comparison state, the performance in terms of achieved MSE training error, error histogram, and regression plots is considered. Firstly, the training MSE error of the 3-18-1 BPNN-PSO-GSA model showed faster convergence than the 3-8-1 BPNN-PSO model, as depicted in Figures 11 and 14. The 3-18-1 structure reached the minimum MSE (1.18  $\times$  10<sup>-7</sup>) in a round of 90 iterations, while 315 iterations were repeated until the 3-8-1 structure reached  $3.14 \times 10^{-3}$ . Secondly, the error histogram of the two best hybrid models also showed significant differences in all phases (training, validation, and testing). Twenty data sets of the 3-18-1 model are located at the zero line (14 for training, 2 for validation, and 4 for testing), as Figure 15 confirms. On the contrary, the 3-8-1 model illustrates that 12 data sets (8 for training, 2 for validation, and 2 for testing) are positioned nearly right to the zero line, and 6 data sets (3 for training, 1 for validation, and 2 for testing) are placed closely at the left as revealed by Figure 11.

Furthermore, the maximum difference in the training phase between actual and predicted surface roughness for the 3-18-1 model (-0.05207 and 0.1093) is smaller than that for the 3-8-1 model (-0.1582 and 0.1954). Thirdly, there was close matching between actual and desired targets in training, validation, testing, and all for the 3-18-1 model (Figure 16) with corresponding *R* values (0.99336, 0.999, 1,

and 0.99475). On the other side, 0.97342, 0.99826, 0.9993, and 0.97997 were recorded as R values of training, validation, testing, and all for the 3–8–1 model, as shown in Figure 13. Therefore, the BPNN–PSO–GSA hybrid model with a 3–18–1 structure was overcome by the 3–8–1 structure of the BPNN–PSO hybrid model in terms of the produced MSE training error, error histogram, and regression plots.

#### 5 Conclusions

This study proposed two aims, namely, to study and optimize the dry-end-milling parameters with an uncoated tool of Ti4Al6V alloy and to investigate the performance of the PSO–GSA hybrid algorithm in training BPNN to predict the surface roughness of the end-milled workpiece. According to the discussion and analysis of the obtained results to achieve the aforementioned two aims, the following points can be concluded:

- 1. The dry-end milling of TiAl4V alloy with an uncoated carbide tool was conducted successfully.
- 2. The parametric study revealed that the generated surface roughness was significantly impacted by the feed rate and depth of cut accompanied by their combined effect, while the cutting speed was not significant.
- 3. The optimization process of dry-end-milling parameters recommends setting the cutting speed at a high level (105 m/min) and feed rate and depth of cut on low levels (0.1 mm/tooth and 1 mm) to produce the minimum surface roughness of 0.49  $\mu m$ .
- 4. The PSO-GSA approved its effectiveness during training and validation of the BPNN compared with the PSO algorithm in terms of the speed convergence, produced error histograms and regression plots.
- 5. The 3–18–1 BPNN–PSO–GSA hybrid model was the best model, where it produced a minimum best MSE of  $3.8 \times 10^{-11}$  compared with  $2.42 \times 10^{-5}$  that corresponds to the 3–8–1 BPNN–PSO model.

**Funding information:** This research received no external funding.

**Author contributions:** Salah Al-Zubaidi: methodology, analysis, supervision, and writing; Jaharah A. Ghani: investigation, supervision, and writing; Che Hassan Che Haron: analysis and writing; Adnan Naji Jameel Al-Tamimi: analysis, writing – review and editing; M.N. Mohammed: writing – review and editing; Alessandro Ruggiero: writing – review

and editing; Samaher M. Sarhan: visualization, writing – review and editing; Oday I. Abdullah: visualization, writing – review and editing; Mohd Shukor Salleh: visualization, writing – review and editing.

**Conflict of interest:** The authors declare that they have no conflict of interest.

#### References

- [1] Su Y, He N, Li L, Li XL. An experimental investigation of effects of cooling/lubrication conditions on tool wear in high-speed end milling of Ti-6Al-4V. Wear. 2006;261(7):760-6.
- [2] Li A, Zhao J, Luo H, Pei Z, Wang Z. Progressive tool failure in high-speed dry milling of Ti-6Al-4V alloy with coated carbide tools. Int J Adv Manuf Technol. 2012;58(5):465–78.
- [3] Elmagrabi N, Che Hassan CH, Jaharah AG, Shuaeib FM. High speed milling of Ti-6Al-4V using coated carbide tools. Eur J Sci. 2008;22(153):153–62.
- [4] Safari H, Sharif S, Izman S, Jafari H. Surface integrity characterization in high-speed dry end milling of Ti-6Al-4V titanium alloy. Int J Adv Manuf Technol. 2015;78(1):651–7.
- [5] Zhao W, Ren F, Iqbal A, Gong L, He N, Xu Q. Effect of liquid nitrogen cooling on surface integrity in cryogenic milling of Ti-6Al-4 V titanium alloy. Int J Adv Manuf Technol. 2020;106(3):1497–508.
- [6] Ahmadi M, Karpat Y, Acar O, Kalay YE. Microstructure effects on process outputs in micro scale milling of heat treated Ti6Al4V titanium alloys. J Mater Process Technol. 2018;252:33–347.
- [7] Mukherjee I, Ray PK. A review of optimization techniques in metal cutting processes. Comput Ind Eng. 2006;50(1):15–34.
- [8] Friaa H, Laroussi Hellara M, Stefanou I, Sab K, Dogui A. Artificial neural networks prediction of in-plane and out-of-plane homogenized coefficients of hollow blocks masonry wall. Meccanica. 2020;55(3):525–45.
- [9] Teng S, Chen G, Gong P, Liu G, Cui F. Structural damage detection using convolutional neural networks combining strain energy and dynamic response. Meccanica. 2020;55(4):945–59.
- [10] Oktem H, Erzurumlu T, Erzincanli F. Prediction of minimum surface roughness in end milling mold parts using neural network and genetic algorithm. Mater Des. 2006;27(9):735–44.
- [11] Bharathi Raja S, Baskar N. Application of particle swarm optimization technique for achieving desired milled surface roughness in minimum machining time. Expert Syst Appl. 2012;39(5):5982–9.
- [12] Del Prete A, De Vitis AA, Anglani A. Roughness improvement in machining operations through coupled metamodel and genetic algorithms technique. Int J Mater Form. 2010;3(suppl 1):467–70.
- [13] Zain AM, Haron H, Sharif S. Integrated ANN-GA for estimating the minimum value for machining performance. Int J Prod Res. 2012;50(1):191–213.
- [14] AL-Khafaji MMH. Neural network modeling of cutting force and chip thickness ratio for turning aluminum alloy 7075-T6. Al-Khwarizmi Eng J. 2018;14(1):67–76.
- [15] Moghri M, Madic M, Omidi M, Farahnakian M. Surface roughness optimization of polyamide-6/Nanoclay nanocomposites using artificial neural network: genetic algorithm approach. Sci World J. 2014;2014:485205.
- [16] Ibraheem MQ. Prediction of cutting force in turning process by using artificial neural network. Al-Khwarizmi Eng J. 2020;16(2):34–46.

- Boga C, Koroglu T. Proper estimation of surface roughness using hybrid intelligence based on artificial neural network and genetic algorithm. J Manuf Process. 2021;70:560-9.
- [18] Rahimi MH, Huynh HN, Altintas Y. On-line chatter detection in milling with hybrid machine learning and physics-based model. CIRP J Manuf Sci Technol. 2021;35:25-40.
- [19] Al-Zubaidi S, A.Ghani J, Che Haron CH, Mohammed MN, Jameel Al-Tamimi AN, M.Sarhan S, et al. Development of hybrid intelligent models for prediction machining performance measure in end milling of Ti6Al4V alloy with PVD coated tool under dry cutting conditions. Lubricants. 2022;10(10):236.
- [20] Kennedy J, Eberhart R. Particle Swarm Optimization. Proceedings of the IEEE International Conference on Neural Networks; 1995 27 Nov-1 Dec; Perth (WA), Australia. IEEE, 2002. p. 1942-8.
- [21] Mirjalili S, Mohd Hashim SZ, Moradian Sardroudi H. Training feedforward neural networks using hybrid particle swarm optimization and gravitational search algorithm. Appl Math Comput. 2012;218(22):11125-37.
- [22] Rashedi E, Nezamabadi-pour H, Saryazdi S. GSA: A gravitational search algorithm. Inf Sci. 2009;179(13):2232-48.
- [23] Ghani JA, Choudhury IA, Masjuki HH. Performance of P10 TiN Coated carbide tools when end milling AISI H13 tool steel at high cutting speed. J Mater Process Technol. 2004;153-154:1062-6.